Crystalline Motion of Interfaces Between Patterns

Andrea Braides
Dipartimento di Matematica, University of Rome Tor Vergata, Italy
Marco Cicalese
Zentrum Mathematik, TU München, Germany
Nung Kwan Yip*
Department of Mathemtics, Purdue University, USA

April 20, 2016

Abstract

We consider the dynamical problem of an antiferromagnetic spin system on a two-dimensional square lattice $\varepsilon\mathbb{Z}^2$ with nearest-neighbour and next-to-nearest neighbour interactions. The key features of the model include the interaction between spatial scale ε and time scale τ, and the incorporation of interfacial boundaries separating regions with microstructures. By employing a discrete-time variational scheme, a limit continuous-time evolution is obtained for a crystal in $\mathbb{R}^2$ which evolves according to some motion by crystalline curvatures. In the case of anti-phase boundaries between striped patterns, a striking phenomenon is the appearance of some "non-local" curvature dependence velocity law reflecting the creation of some defect structure on the interface at the discrete level.

Keywords: antiferromagnetic spin system, anti-phase boundaries, microstructures, defects, interface motion, crystalline curvature motion

1 Introduction

The modeling of realistic behavior of materials is dictated by the ubiquitous presence of defects. The dynamics of these defects is controlled by both the energetic and kinematic information. The former determines the structures or more accurately, *micro-structures* of the defects while the latter is related to the *dissipation* mechanism. It can be a challenge to characterize these concepts quantitatively and most important, relate the microscopic and macroscopic measurable quantities. On the other hand, variational principles play an important role as materials often try to minimize some underlying energy. Based on such considerations, many mathematical formulations have been constructed to model the structure and dynamics of defects. The current paper provides such an example starting from lattice interactions.

A simple model to capture the appearance of microstructures in energy-driven systems involves competing short-range and long-range energies as in the Ising models considered in [23, 24] (see also the references therein) where ferromagnetic short range interactions compete with anti-ferromagnetic long-range interactions. We here consider a simple model in which the competition mechanism is achieved in an antiferromagnetic spin system on a square lattice. In this case, if nearest-neighbour (NN) and next-to-nearest neighbour

*Corresponding author: email: yip@math.purdue.edu; phone: 1-(765)-494-1941; fax: 1-(765)-494-0548

(NNN) interactions are taken into account, the system may exhibit *ground states – global energy minimizing states* – consisting of non-trivial patterns which cannot be reduced to a trivial ferromagnetic description via a change of variables. Contrary to the continuum setting, the lattice framework allows us to describe in a precise way the interactions between different types of microstructures. The model we consider leads to two lattice spacings periodic horizontal and vertical stripes as ground states. Taking into account the possibility of *phase boundaries* between stripes of different orientations and of *anti-phase boundaries* between stripes of the same orientation, the interactions between the ground states can be described through a continuum approximation by an *interfacial energy* between regions taking values in the four phases: the horizontal and vertical stripes and their shifted versions. This discrete-to-continuum approach has been analyzed in [1] by an appropriate limit procedure using the framework of Γ-convergence. This continuum approximation also allows to describe the discrete optimal configurations for a class of static problems (see [9] for a more general result on systems with patterns and modulated phases using the same approach).

The appearance of interfacial energies as an approximation of spin energies suggests the possibility of a continuum description of dynamical problems in terms of geometric motions of interfaces. In the case of ferromagnetic energies for which no microstructure arises, the continuum description involves only two homogeneous phases and a crystalline perimeter energy (see [1, 13] for a variational formulation). For general perimeter energies, a variational Euler scheme has been introduced by Almgren, Taylor and Wang [4] and Luckhaus-Sturzenhecker [30] which show how motions by mean-curvature can be obtained as a form of gradient flow of such perimeters. The work [3] by Almgren and Taylor treats the case of crystalline mean-curvature flows. This Euler scheme leads to an implicit-time discretization procedure producing a discrete-time evolution parameterized by a time-step τ. The limit motion is subsequently obtained by letting $\tau \to 0$. This approach to construct gradient-flow type evolutions has been subsequently formalized in a more abstract setting under the label of *minimizing movements* by De Giorgi (see [5]): at each time scale τ, the discrete-time motions $\{u_k\} = \{u_k^\tau\}$ are obtained by successive minimization of a total energy of the type

$$F_\tau(u) = E(u) + \frac{1}{\tau} D(u, u_{k-1}), \tag{1.1}$$

where E is interpreted as an energy and D as a dissipation. The latter can also be viewed as some penalty term to restrict appropriately the motion from u_{k-1} to u_k. In [4, 30] and [3], the variable u is a set, $E(u)$ is its euclidean and crystalline perimeter, respectively, and $D(u, u_{k-1})$ accounts for the distance between the boundaries of u and u_{k-1}.

If we try to apply the above scheme to spin systems, two issues arise. The **first** is due to the interaction between the lattice *space scale* ε and the *time scale* τ. The latter is related to the typical velocity at which the motion takes place. Indeed, at very slow time-scales; i.e., when τ is very small, the energy barriers of F_τ (or more accurately, now it should be written as $F_{\varepsilon,\tau}$) are at least of order ε and hence they forbid any transition from one state (*local minima*) to another. The discrete-time motions are thus constant, giving rise to a continuum *pinned state*. Conversely, when ε is very small, local minima can be overcome and then the motion is asymptotically close to the minimizing movement of the continuum energy obtained by Γ-convergence. However, this motion is often too coarse to reveal any effects coming from *local minimization*. Instead, the most relevant and interesting *effective motion* seems to be the one in which the two scales interact; more precisely, when $\tau \sim \varepsilon$. The previous two extreme cases (pinning and motion according to the Γ-limit) can then be obtained as a by-product. In a paper by Braides, Gelli and Novaga [10], a description is given for the effective continuum motion of ferromagnetic systems, showing new phenomena such as pinning only for large sets, non-uniqueness of motions, and quantization of the energy. These results have been further analyzed in a paper by Braides and Scilla [11] showing that different velocity laws can be obtained for systems with the same static behaviour. These works thus highlight the role of local minimization in the computation of a *curvature-dependent homogenized velocity*. In both papers [10, 11], the effective motion is computed by a diagonal argument in the minimizing-movement scheme. The continuous-time limit depends on the precise τ-ε asymptotics of the discrete-time motions $\{u_k\} = \{u_k^{\tau,\varepsilon}\}$ which live at space scale ε and time scale τ and are obtained by successive minimization of a total energy of the type

$$F_{\varepsilon,\tau}(u) = E_\varepsilon(u) + \frac{1}{\tau} D_\varepsilon(u, u_{k-1}). \tag{1.2}$$

The general properties of *minimizing movements along a sequence of energies at given time scale* are studied in [8]. In [10] and [11] $u_k^{\tau,\varepsilon}$, are subsets of $\varepsilon\mathbb{Z}^2$ considered as a discretization of continuum sets.

As a **second** issue, we face the problem of giving continuum descriptions when the spin system develops *microstructures*, in particular, a spin system with next-to-nearest neighbour interaction (NNN). For the model we consider, a limit system is in general described by the four phases labelled by $\pm e_1$ (the two modulated phases with vertical stripes) and $\pm e_2$ (the two modulated phases with horizontal stripes). In this case, a minimizing movement should be described by the evolution of a *network system* representing the boundaries of multi-phase regions. Unfortunately, even in the continuum case when the interfacial energy is simply given by the usual euclidean length, the theory of the evolution of such a system is not fully developed (see [29, 32, 31, 36] for some results). Thus in this work, we consider the particular case of the motion of a *single crystal* so that we just need to analyze the geometric motion of a single interface. In Fig. 1 we have pictured typical crystals between different phases. The figure also highlights how the overall shape of the crystal and the structure of the interfaces are dictated by the phases both inside and outside of the crystal.

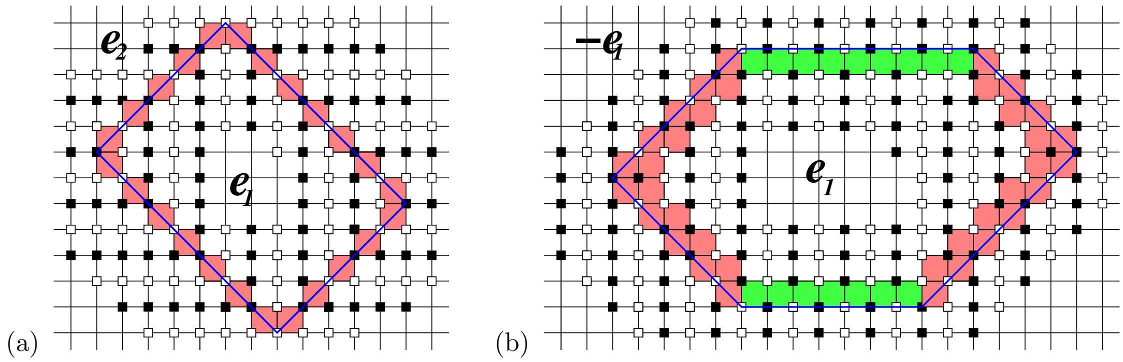

Figure 1: Wulff-like crystals: (a) between e_1 phase (vertical stripes) and e_2 phase (horizontal stripes); (b) between e_1 phase and $-e_1$ phase. Note that the $-e_1$ phase is the e_1 phase shifted by one lattice spacing.

Our results resemble those obtained by Almgren and Taylor in [3] but incorporate several new features. To highlight them, we point out here that the most complex and interesting case is that of a crystal evolving in a matrix of the same pattern, incorporating the presence of *anti-phase boundaries*. Without loss of generality, we consider the case of an e_1-crystal in a $-e_1$-matrix. In this case, the Wulff shape for the corresponding continuum energy is an irregular convex hexagon with two horizontal sides and the other four oriented along the bisectric directions; i.e., with slopes ± 1. The corresponding microscopic picture involves defect structures in addition to the ground states (Fig. 1(b)). We study a minimizing-movement scheme with a dissipation term D_ε analogous to that of [3]. In our scheme, the distance between two discrete crystals accounts for the number of square cells on which the pattern changes from one configuration to another.

One of the major challenges is to show that during each minimization step we can still recognize an e_1-crystal in a $-e_1$-matrix. To that end, we remark that it is sufficient to consider only initial data which are “Wulff-like” as illustrated in Fig. 1(b); i.e., discrete sets corresponding to arbitrary convex hexagons with sides having the same orientations as those of a Wulff shape. Indeed, the extension to more general initial shapes is already illustrated in [10]. For such a Wulff-like initial data, all the sets obtained in the Euler scheme can be shown to be Wulff-like. Thus the description of their dynamical behaviour can be reduced to a system of ordinary differential equations describing the evolution of the sides. The relevant regime for the asymptotic analysis turns out to be $\varepsilon = \tau$ (or more generally, $\varepsilon/\tau \to \alpha$). A first effect due to the spatial discreteness is the fact that the symmetries of the dissipation term are different from those of the Wulff shape, leading to a *mobility effect* analogous to the one obtained following the approach in [3]. In order to take this effect into account, we have a different scaling in the crystalline curvature κ for the different sides. (Following the continuum description in [38], crystalline curvature of a side is taken to be inversely proportional to its length.) With this normalization in mind, the velocity of each horizontal side of the crystal along the inward normal direction is simply given by

$$V = V(\kappa) = \lfloor \kappa \rfloor, \tag{1.3}$$

where the integer part is due to the fact that a side can move only by discrete steps analogously as in [10].

A second, more striking effect is in the description of the motion of the bisectic sides, each of which moves with a velocity function

$$V = V(\kappa, \kappa'), \tag{1.4}$$

which depend on *both* κ, the curvature of itself and also κ', the curvature of its bisectric neighbour. This is due to a new phenomenon at the discrete level. Indeed, in two successive steps of the Euler scheme, a pair of

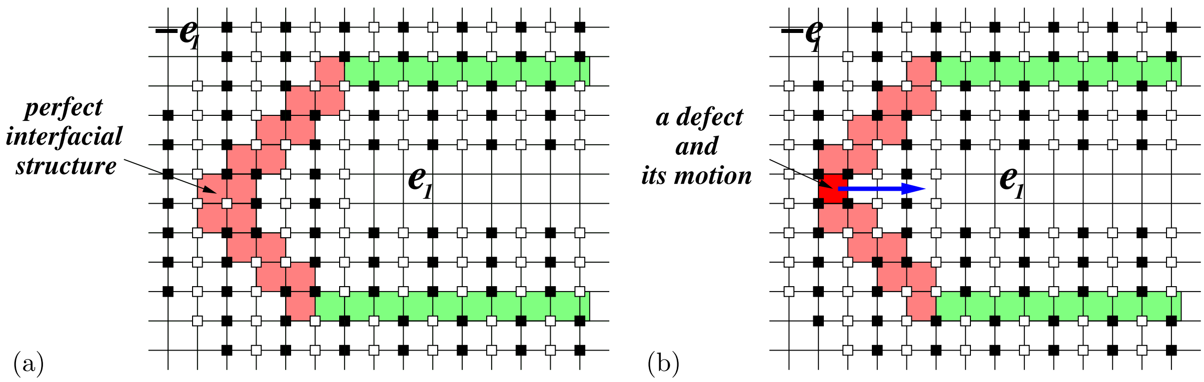

Figure 2: Motion by the creation of defects. A perfect interfacial structure in (a) and the presence of a defect and its motion in (b).

neighbouring bisectrix sides may move maintaining a ‘perfect’ shape, as that in Fig. 2(a), or create a ‘defect’ at the vertex (see Fig. 2(b)). The optimality of either of the two options depends simultaneously on the (inverse of the) length of both sides, and hence on the two curvatures. This new effect shows that minimizing movements of spin energies not only can lead to a complex dependence of the velocity on the crystalline curvature due to some homogenization phenomena, but may also generate some “non-local” effects due to the competition between interfacial microstructures. Note that this phenomenon is different from the creation of bulk microstructure, as in the formation of mushy layers in high-contrast spin systems [12].

It is instructive to compare our results to those interfacial motions obtained from spin systems which are more related to Statistical Mechanics. Two examples are the Glauber and Kawasaki dynamics. Note that a key feature of our current problem, due to the spatial and temporal discretization, is the presence of a large number of local minima on the underlying energy landscape. A discrete-time variational scheme is employed to overcome these local minima. This is reminiscent to adding thermal noise or stochastic fluctuations. As mentioned earlier, the most interesting regime is the critical case, $\varepsilon = \tau$ in which the size of the noise and the depth of local minima are compatible. Otherwise, either the discrete nature of the problem will disappear (if the noise it too big) or the evolution will be completely pinned (if the noise is too small). On the other hand, the existing works [17, 18, 21, 22, 26, 27, 28] on the connection between interfacial motions and stochastic Ising models or interactive particle systems mostly involve long range spatial interactions or fast spin-exchange mechanism so that sufficient sampling and averaging of the energy landscape occurs. Such a procedure in essence eliminates all the effects coming from local minimization. On the continuum level, a very important example is the Allen-Cahn or the Modica-Mortola functional [2, 33, 35]. Its gradient flow is shown to be related to motion by mean curvature [20, 16, 19, 25]. These works again do not incorporate any underlying discrete and fine-scale structures. In a general setting, the work [34] gives sufficient conditions for the convergence of dynamics when the energy landscape converges. However, the framework currently also overlook any fine scale structures. In a stationary setting, the work [6] illustrates the interaction between interfacial thickness and the underlying spatial microstructures. Overall, it is interesting to formulate and understand more quantitatively the effects of noise on the effective dynamics when underlying fine scale structures are present.

Another extension of the current setting is the consideration of multi-phase regions. Recall that the current antiferromagnetic system have four ground states $\pm e_1$ and $\pm e_2$. Their co-existence can lead to triple- or quadruple junctions. The works [14, 15] provides further examples demonstrating the appearances of junctions and interfaces between spatially modulated patterns. The dynamics of these systems have not been fully analyzed. See however [39] for the introduction of a general framework, using again some variational time-discretization scheme.

The outline of this paper is as follows. In Section 2, we describe the setting of the spin system, introduce the ground states and the discrete-time variational scheme, and then give the statements of our results. In Section 3, we prove the optimality properties of discrete Wulff shapes or Wulff-like envelopes. In Section 4, we prove the continuum limit of the motion laws for a Wulff-like (rectangular) e_1-crystal inside an e_2-matrix. Section 5, which is the most technical part of this paper, proves the continuum description of the motion of a Wulff-like (hexagonal) e_1-crystal inside an $-e_1$-matrix.

2 Problem Setting

In this section, we introduce the machinery needed for our results. It is divided into stationary and dynamic considerations.

2.1 Analysis of Patterns - Stationary Case

We consider the energy defined on a two-dimensional spin system on $\varepsilon\mathbb{Z}^2$ studied by Alicandro, Braides and Cicalese [1] of the following form

$$\begin{aligned} E_\varepsilon(u) &= c_1 \sum_{\mathrm{NN}} \varepsilon^2 u_i u_j + c_2 \sum_{\mathrm{NNN}} \varepsilon^2 u_i u_j \\ &= \sum_{\{i,j,k,l\}} \frac{c_1}{2} \varepsilon^2 (u_i u_j + u_j u_k + u_k u_l + u_l u_i) + c_2 \varepsilon^2 (u_i u_k + u_j u_l) \end{aligned} \tag{2.1}$$

where the subscripts NN and NNN refer to summation over *nearest neighbours* (i.e., $i,j \in \varepsilon\mathbb{Z}^2$ with $|i-j| = \varepsilon$) and *next-to-nearest neighbours* (i.e., $i,j \in \varepsilon\mathbb{Z}^2$ with $|i-j| = \varepsilon\sqrt{2}$), respectively, and the indices $\{i,j,k,l\}$ denote the vertices in $\varepsilon\mathbb{Z}^2$ of a square starting from the lower left vertex and continuing in the counter-clockwise manner (see Fig. 3(a)). In the formula above, u is a spin function taking values in $\{-1,1\}$. Note

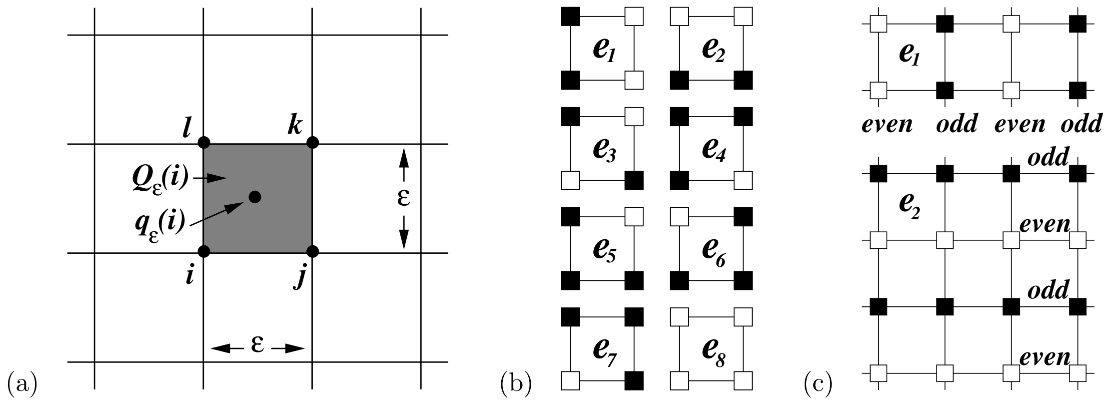

Figure 3: Grid and patterns. (a) Vertices, cubes, and centers; (b) The patterns $e_1, e_2, \ldots, e_8$; (c) The two-periodic tessellation e_1 and e_2. In the figure, ■ $= -1$, and □ $= +1$.

that it will be necessary to renormalize the energy so as to avoid the value $-\infty$. This will be done by suitably rewriting the energy and subtracting the energy of a ground state.

For convenience, we introduce the following notation:

$$\begin{aligned}
\mathcal{S}_\varepsilon &= \left\{u : \varepsilon\mathbb{Z}^2 \longrightarrow \{-1,1\}\right\} && (2.2)\\
A &= (x_A, y_A), \quad \text{for } A \in \varepsilon\mathbb{Z}^2 && (2.3)\\
Q_\varepsilon(i) &= i + \varepsilon[0,1]^2, \quad \text{for} \quad i \in \varepsilon\mathbb{Z}^2 && (2.4)\\
q_\varepsilon(Q_\varepsilon(i)) &= i + \varepsilon\left(\frac{1}{2}, \frac{1}{2}\right) \quad (= \text{center of } Q_\varepsilon(i)) && (2.5)\\
\mathcal{Q}_\varepsilon &= \left\{Q_\varepsilon(i) : i \in \varepsilon\mathbb{Z}^2\right\}. && (2.6)
\end{aligned}$$

If no confusion arises, we will use the simplified notation:

$$Q_\varepsilon = Q_\varepsilon(q_\varepsilon) := Q_\varepsilon(i), \quad \text{and} \quad q_\varepsilon = q_\varepsilon(i) := q_\varepsilon(Q_\varepsilon).$$

We further define the *cell patterns* as follows.

Definition 2.1 (Cell Patterns)**.** *Let* $\mathcal{P} = \{\pm e_1, \pm e_2, \ldots, \pm e_8\}$ *where*

$$\begin{aligned}
&e_1 = (-1,1,1,-1), \quad && e_2 = (-1,-1,1,1),\\
&e_3 = (1,-1,1,-1), \quad && e_4 = (-1,1,-1,-1),\\
&e_5 = (-1,-1,1,-1), \quad && e_6 = (-1,-1,-1,1),\\
&e_7 = (1,-1,-1,-1), \quad && e_8 = (1,1,1,1).
\end{aligned} \tag{2.7}$$

(See Fig. 3(b)*.) For simplicity, in the following, we will use* e^3 *to refer to any element in* $\{\pm e_4, \pm e_5, \pm e_6, \pm e_7\}$ *which are patterns consisting of "three of a kind"; i.e.,*

$$w = e^3 \Longleftrightarrow w \in \{\pm e_4, \pm e_5, \pm e_6, \pm e_7\}. \tag{2.8}$$

In addition, unless the sign is explicitly needed, we employ the following convention:

$$w = e_3 \Longleftrightarrow w \in \{\pm e_3\}\,,\ \ w = e_8 \Longleftrightarrow w \in \{\pm e_8\}\,. \tag{2.9}$$

The above notation is used since our subsequent analysis treats $+e_3$ and $+e_8$ the same as $-e_3$ and $-e_8$.

For any $u \in \mathcal{S}_\varepsilon$, $w = w(u)$ denotes the $\mathcal{P}$-valued function:

$$w = w(u) : \mathcal{Q}_\varepsilon \longrightarrow \mathcal{P}, \qquad w(u)(Q_\varepsilon(i)) = (u_i, u_j, u_k, u_l). \tag{2.10}$$

In addition, we introduce

$$\widetilde{\mathcal{W}}_\varepsilon = \{w : \mathcal{Q}_\varepsilon \longrightarrow \mathcal{P}\}\,, \tag{2.11}$$

$$\mathcal{W}_\varepsilon = \left\{w \in \widetilde{\mathcal{W}}_\varepsilon : w(Q_\varepsilon(i)) = (u_i, u_j, u_k, u_l) \text{ for some } u \in \mathcal{S}_\varepsilon \text{ and all } i \in \varepsilon\mathbb{Z}^2\right\} \tag{2.12}$$

to denote the collection of arbitrary pattern-valued functions and those which can be actually achieved by a spin function. Since we will use these spaces with fixed $\varepsilon > 0$, we will drop the subscript ε in the notation; i.e., we will write $\widetilde{\mathcal{W}}$ and $\mathcal{W}$ in the place of $\widetilde{\mathcal{W}}_\varepsilon$ and $\mathcal{W}_\varepsilon$.

For simplicity, we often write $w(Q_\varepsilon(i))$ as $w(i)$ or $w(u)_i$. Note that $\mathcal{W} \subsetneqq \widetilde{\mathcal{W}}$. In the intermediate steps of our proof, we often find it easier to manipulate $\mathcal{P}$-valued functions $\widetilde{w} \in \widetilde{\mathcal{W}}$. In the very last step, we will then show that in fact $\widetilde{w} = w(u)$ for some $u \in \mathcal{S}_\varepsilon$.

In principle, (u_i, u_j, u_k, u_l) can take arbitrary values. However we are actually interested in *spatially periodic patterns*, or *tessellation*, in particular those formed by $\pm e_1$ and $\pm e_2$. Note that in order to form a striped pattern as in Fig. 3(c), both e_1 and $-e_1$ are needed to form a tessellation which is a *two-periodic pattern*. The same is true for e_2 and $-e_2$. We hereby give the following definition.

Definition 2.2. *Let $Q_\varepsilon(i)$ be a square with $i = (x_i, y_i) \in \varepsilon\mathbb{Z}^2$ and $w(i) \in \mathcal{P}$. We say,*

$$w(i) \in [e_1] \text{ (resp., } \in [-e_1]) \quad \text{if } w(i) = \begin{cases} e_1 & \text{if } \frac{x_i}{\varepsilon} \text{ is even (resp., odd)} \\ -e_1 & \text{if } \frac{x_i}{\varepsilon} \text{ is odd (resp., even),} \end{cases} \tag{2.13}$$

$$w(i) \in [e_2] \text{ (resp., } \in [-e_2]) \quad \text{if } w(i) = \begin{cases} e_2 & \text{if } \frac{y_i}{\varepsilon} \text{ is even (resp., odd)} \\ -e_2 & \text{if } \frac{y_i}{\varepsilon} \text{ is odd (resp., even);} \end{cases} \tag{2.14}$$

i.e., we identify a 2ε-periodic pattern with its trace on $Q_\varepsilon(0)$.

For simplicity, for $p = 1, 2$, we use "$w = \pm e_p$" to indicate "$w \in [\pm e_p]$".

Complementary to the one above, we give the following definition which will be used in several places of our proofs.

Definition 2.3. *An ordered pair $(m, n) \in \mathbb{Z}^2$ is said to have* even *or* odd parity *if $m + n$ is an even or odd integer. This is denoted by* $\mathrm{Par}(m + n) = 0$ *or* 1.

A point $A = (x_A, y_A) \in \varepsilon\mathbb{Z}^2$ is said to have even *or* odd parity *if $(X_A, Y_A) := (\frac{x_A}{\varepsilon}, \frac{y_A}{\varepsilon}) \in \mathbb{Z}^2$ has even or odd parity. For simplicity, we will also use the convention* $\mathrm{Par}(x_A + y_A) = 0$ *or* 1.

In this paper, we will always assume

$$c_1 > 0,\ c_2 > 0, \text{ and } 2c_2 > c_1 \tag{\textbf{H1}}$$

in which case the *ground states*, or the *energy minimizing patterns*, are the two-periodic patterns $\pm e_1$ and $\pm e_2$. The case $2c_2 < c_1$ can in fact be transformed to the ferromagnetic case. In addition, we will impose the condition **(H2)** in Section 2.3. See [1, Section 5] and Section 2.4 for more discussion concerning these conditions.

In order to analyze the interfacial energy between the ground states, we consider the following functional,

$$E_\varepsilon^{(1)}(u) = \sum_{\{i,j,k,l\}} \varepsilon \frac{c_1}{2}(u_i u_j + u_j u_k + u_k u_l + u_l u_i) + \varepsilon c_2(u_i u_k + u_j u_l + 2). \tag{2.15}$$

Compared with (2.1), the energy written in this way is always positive, thus avoiding the $-\infty$ and $+\infty$ indeterminacies, and it is normalized so that ground states have zero energy. Moreover it is scaled by ε so that it behaves as a surface energy.

Using the notation of w and e_i's, $E_\varepsilon^{(1)}$ can be conveniently written as

$$E_\varepsilon^{(1)}(u) = \varepsilon \sum_{i \in \varepsilon\mathbb{Z}^2} f(w(u)_i) \tag{2.16}$$

where $f : \mathcal{P} \longrightarrow \mathbb{R}$ is defined as:

$$f(w) = \begin{cases} 0 & \text{if } w \in \{\pm e_1, \pm e_2\} \\ 4c_2 - 2c_1 & \text{if } w \in \{\pm e_3\}, \\ 2c_2 & \text{if } w = e^3; \text{i.e., } w \in \{\pm e_4, \pm e_5, \pm e_6, \pm e_7\}, \\ 4c_2 + 2c_1 & \text{if } w \in \{\pm e_8\}. \end{cases} \tag{2.17}$$

Note that $f(w) \geq 0$, and $f(w) = 0$ only if $w \in \{\pm e_1, \pm e_2\}$.

A central information is the *minimum energy* and the *minimizing interfacial structure* connecting two ground states, for which the following simple lemma contains the essential ingredients. We omit the proof due to its simplicity.

Lemma 2.4 (Slicing estimates in the vertical and horizontal directions ([1] Section 5))**.** *Let $A, B, C, D \in \varepsilon\mathbb{Z}^2$ be such that AB and CD are two horizontal segments of length ε and $ABDC$ encloses a rectangle Ω. In other words,*

$$x_B = x_A + \varepsilon,\ y_B = y_A,\ x_D = x_C + \varepsilon,\ y_D = y_C,\ x_C = x_A,\ \text{ and } y_C - y_A \geq \varepsilon.$$

For any $u \in \mathcal{S}_\varepsilon$, denote

$$E_\varepsilon^{(1)}(u, \Omega) = \varepsilon \sum_{\{i \in \varepsilon\mathbb{Z}^2 : Q_\varepsilon(i) \subseteq \Omega\}} f(w(u)_i).$$

Then the following statements hold.

1. *Suppose $u(A) = u(B)$ and $u(C) = u(D)$. If $u(A) = u(C)$ and $y_C - y_A$ is an odd multiple of ε or if $u(A) \neq u(C)$ and $y_C - y_A$ is an even multiple of ε, then*

$$E_\varepsilon^{(1)}(u, \Omega) \geq 2f(e^3)\varepsilon = 4c_2\varepsilon. \tag{2.18}$$

2. *Suppose $u(A) = u(B)$ and $u(C) \neq u(D)$ or $u(A) \neq u(B)$ and $u(C) = u(D)$. Then*

$$E_\varepsilon^{(1)}(u, \Omega) \geq f(e^3)\varepsilon = 2c_2\varepsilon. \tag{2.19}$$

3. *Suppose $u(A) \neq u(B)$, $u(C) \neq u(D)$, and $u(A) \neq u(C)$. Then*

$$E_\varepsilon^{(1)}(u, \Omega) \geq f(e_3)\varepsilon = (4c_2 - 2c_1)\varepsilon. \tag{2.20}$$

The above are called slicing estimates in the vertical direction. *Similar conclusions hold when AB and CD form vertical segments. Then the statements are called slicing estimates in the* horizontal direction.

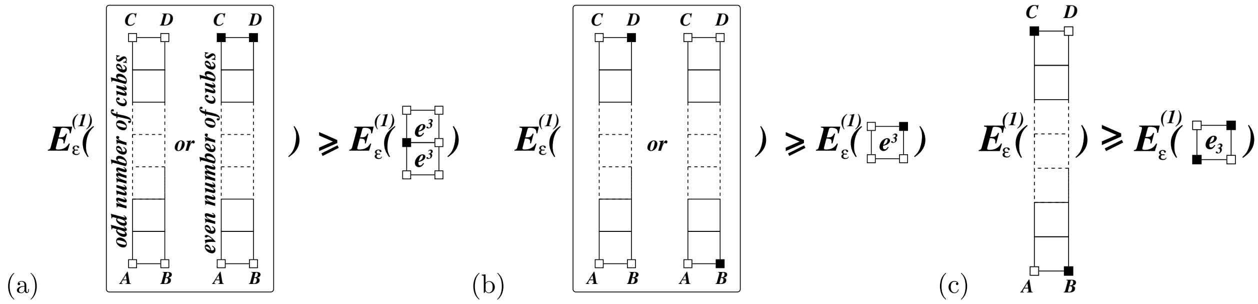

Figure 4: Slicing estimates and minimizing structures in the vertical directions: (a) for (2.18); (b) for (2.19); (c) for (2.20). The illustration for horizontal slicing estimates are similar.

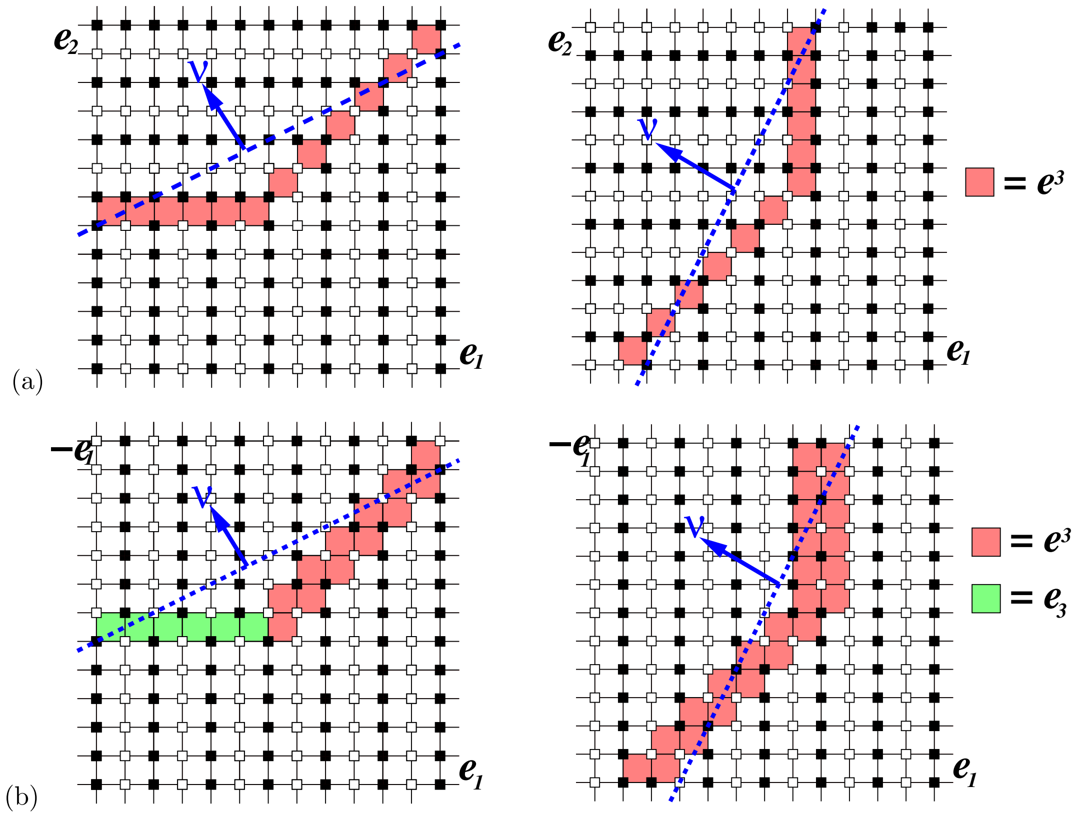

Figure 5: Minimizing interfacial patterns between: (a) e_1 and e_2, and (b) e_1 and $-e_1$ in different directions. The interfaces (dotted lines) and their normal vectors (ν) are also indicated in the figures.

We illustrate the lemma above in Fig. 4 in which the patterns attaining the minimum energy values are also shown.

Using the lemma, it was deduced in [1] that the minimizing interfacial structures between $\pm e_1$ and $\pm e_2$ is that illustrated in Figure 5(a) while that between e_1 and $-e_1$ is that illustrated in Figure 5(b). Note that the structure of the interface depends not only on the normal direction but also on the patterns across the interface: the one in (a) consists of only e^3 while the one in (b) consists of both e^3 and $\pm e_3$.

In the continuum description, it is proved in [1] that $E_\varepsilon^{(1)}$ Γ-converges with respect to the $L^1_{\rm loc}$-topology to the functional $F : L^1_{\mathrm{loc}}(\mathbb{R}^2; \mathcal{P}) \to \mathbb{R} \cup \{+\infty\}$ defined as

$$F(w) = \begin{cases} \displaystyle\int_{S(w)} \varphi(w^+, w^-, \nu_w) d\mathcal{H}^1, & w \in BV_{\mathrm{loc}}(\mathbb{R}^2; \{\pm e_1, \pm e_2\}), \\ +\infty, & \text{otherwise,} \end{cases}$$

where $S(w)$ denotes the jump set of w and $\varphi : \{\pm e_1, \pm e_2\} \times S^1 \to \mathbb{R}^+$ is defined as follows:

$$\begin{aligned} \varphi(\pm e_1, \pm e_2, \nu) &= 2c_2(|\nu_1| \vee |\nu_2|), \\ \varphi(\pm e_1, \mp e_1, \nu) &= 4c_2|\nu_1| + (4c_2 - 2c_1)(|\nu_2| - |\nu_1|)^+, \\ \varphi(\pm e_2, \mp e_2, \nu) &= 4c_2|\nu_2| + (4c_2 - 2c_1)(|\nu_1| - |\nu_2|)^+. \end{aligned}$$

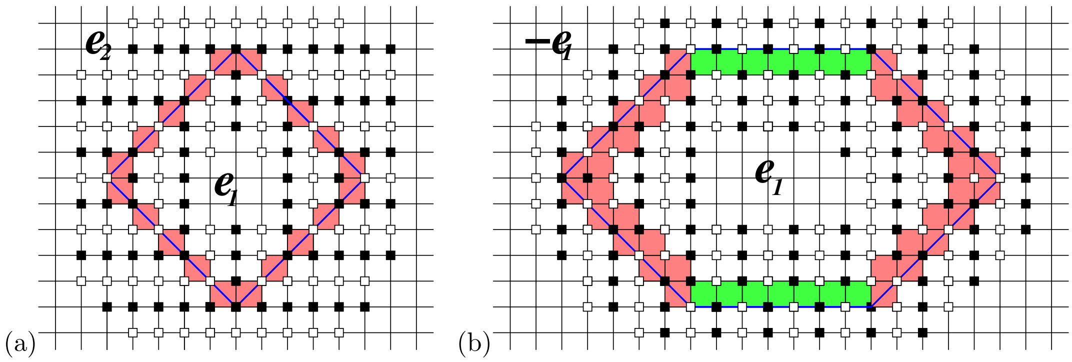

Figure 6: Wulff shapes for (a) $\psi_1(\nu)$ and (b) $\psi_2(\nu)$

For the remaining part of this paper, we will use $\psi_1(\cdot)$ to denote $\varphi(e_1, e_2, \cdot)$, the interfacial density between e_1 and e_2, and $\psi_2(\cdot)$ to denote $\varphi(e_1, -e_1, \cdot)$, the interfacial density between e_1 and $-e_1$. Then at the continuum level, the Wulff shape; i.e., *the shape with the smallest interfacial energy for given area* is a square with the sides pointing along the bisectrix direction[1] for ψ_1, (Figure 6(a)) while it is a hexagon-like polygon formed by two horizontal and four bisectrix segments for ψ_2 (Figure 6(b)). For convenience, we call the former a *bisectic-square* and the latter a *bisectrix-hexagon*. However, at the discrete level, this description is not complete. This will be elaborated in Section 3.

2.2 Discrete-Time Variational Scheme - An Approach to Dynamics

In the spirit of [10] we will consider the continuous motion derived from applying to the energy $E_\varepsilon^{(1)}$ the "minimizing movement" scheme introduced by Almgren, Taylor and Wang [4] and Luckhaus and Sturzenhecker [30]: given any $u^0 \in \mathcal{S}_\varepsilon$, we will construct $\left\{u^k \in \mathcal{S}_\varepsilon\right\}_{k=1}^\infty$ obtained from a miminization process. Each step approximates some crystalline motion by mean curvature. Then we will investigate the limit(s) as $\varepsilon,\ \tau \longrightarrow 0$.

For concreteness, we consider the motion of a single crystal consisting of e_1. For this, we give the following definitions.

[1]A bisectrix direction has slope ± 1. A bisectrix segment is a segment along the bisectrix direction.

Definition 2.5. *Let* $w^\infty \in \{e_2, -e_1\}$ *denote the* exterior phase *(or* far-field condition*). We define*

$$\begin{aligned} S_\varepsilon^\infty &= \left\{u \in \mathcal{S}_\varepsilon,\ w(u)_i = w^\infty \text{ for } i \text{ outside some bounded subset of } \varepsilon\mathbb{Z}^2.\right\} && (2.21)\\ K_u &= \bigcup \{Q_\varepsilon(i) : w(u)_i = e_1\} \quad (e_1\text{-crystal}). && (2.22)\\ \partial_\varepsilon K_u &= \bigcup \left\{Q_\varepsilon(i) : w(u)_i \notin \{e_1, w^\infty\}\right\} \quad (\text{interfacial region}). && (2.23)\end{aligned}$$

Definition 2.6. *Let* $\|z\|_1 = |z_1| + |z_2|$ *for* $z = (z_1, z_2) \in \mathbb{R}^2$*. Define:*

1. *for* $i, j \in \varepsilon\mathbb{Z}^2$, $\mathrm{Dist}^1_\varepsilon(Q_\varepsilon(i), Q_\varepsilon(j)) = \|q_\varepsilon(i) - q_\varepsilon(j)\|_1$*;*
2. *for* $A, B \subseteq \mathcal{Q}_\varepsilon$, $\mathrm{Dist}^1_\varepsilon(A, B) = \inf\{\|q_\varepsilon(i) - q_\varepsilon(j)\|_1,\ q_\varepsilon(i) \in A,\ q_\varepsilon(j) \in B\}$.

Our time-discrete variational scheme is defined using the functional $\mathcal{F}_{\varepsilon,\tau} : \mathcal{S}_\varepsilon^\infty \times \mathcal{S}_\varepsilon^\infty \longrightarrow \mathbb{R}_+$:

$$\mathcal{F}_{\varepsilon,\tau}(u, v) = E_\varepsilon^{(1)}(v) + \frac{\varepsilon^2}{\tau} \sum_{\{i\in\varepsilon\mathbb{Z}^2:\ w(v)_i \neq w(u)_i\}} \mathrm{Dist}^1_\varepsilon(Q_\varepsilon(i), \partial_\varepsilon K_u). \tag{2.24}$$

The functional above can also be written in the equivalent form

$$\mathcal{F}_{\varepsilon,\tau}(u, v) = E_\varepsilon^{(1)}(v) + \frac{1}{\tau} \int_{\{\bigcup Q_\varepsilon(i):\ w(v)_i \neq w(u)_i\}} \mathrm{Dist}^1_\varepsilon(x, \partial_\varepsilon K_u)\, dx \tag{2.25}$$

reminiscent to the functional used in [4], where

$$\mathrm{Dist}^1_\varepsilon(x, \partial_\varepsilon K_u) = \inf\{\|q_\varepsilon(i) - q_\varepsilon(j)\|_1,\ x \in q_\varepsilon(i),\ q_\varepsilon(j) \subset \partial_\varepsilon K_u\}.$$

The first part of $\mathcal{F}_{\varepsilon,\tau}$ is the interfacial energy $E_\varepsilon^{(1)}$ while the second is called the *incremental bulk term* $B_{\varepsilon,\tau}$ or *dissipation*. The intuition behind $\mathcal{F}_{\varepsilon,\tau}$ is that given u, minimizing $\mathcal{F}_{\varepsilon,\tau}(u, \cdot)$ is to reduce $E_\varepsilon^{(1)}$ as much as possible but with the movement limited by $B_{\varepsilon,\tau}$. Our time variational scheme produces $\left\{u_\tau^k, K_\tau^k : k = 1, 2, \ldots\right\}$ obtained by successive minimizations:

$$u_\tau^{k+1} \in \operatorname{argmin}\left\{\mathcal{F}_{\varepsilon,\tau}(u_\tau^k, v)\right\} \quad \text{and} \quad K_\tau^k = K_{u_\tau^k}. \tag{2.26}$$

Each minimization step can be shown to approximate some kind of curvature motion. We remark that the mobility of the interface is directly linked to the choice of the distance function. The L^1-distance function defined above simplifies many of the computation in this paper but in principle other distance functions, such as the L^∞-distance, can also be used.

From general compactness arguments, it is possible to show that upon taking the limit $\varepsilon \to 0$ and $\tau = \tau(\varepsilon) \to 0$, then up to subsequence, the piecewise-constant scaled interpolations $u_\tau(t) = u_\tau^{\lfloor t/\tau \rfloor}$ defined for $t \geq 0$ converge uniformly to a function $u : [0, +\infty) \to BV_{\mathrm{loc}}(\mathbb{R}^2; \{\pm e_1, \pm e_2\})$ which is called a *minimizing movement along* $E_\varepsilon^{(1)}$ at scale τ [8].

Our main results concern the characterization of such u. The statements depend on the relative rate of ε, τ going to zero and also on whether the interface is between e_1 and e_2, or e_1 and $-e_1$. We will show that in fact $u \in BV_{\mathrm{loc}}(\mathbb{R}^2; \{e_1, w^\infty\})$ and the minimizing movement is described as a crystalline-type motion of the set $D(t)$ obtained as limit of the time-discrete interpolations $K_{u_\tau^{\lfloor t/\tau \rfloor}}$

In the continuous space setting, the above scheme has been implemented to produce an existence theorem for mean-curvature flow. Specifically, with a suitably chosen distance function (which is simply the usual euclidean distance function), if the interfacial energy $E_\varepsilon^{(1)}$ is given by some euclidean or crystalline perimeter functional independent of ε, the scheme has been shown rigorously to produce anisotropic [4, 30] or crystalline curvature motions [3], respectively. For an overview of crystalline motion, we refer to [37, 38], in particular for a discussion of the concepts surface energy, Wulff shape, distance and mobility functions. For an analysis of results in the case of general ε-dependence energies $E_\varepsilon^{(1)}$, we refer to [8].

2.3 Statement of Main Results

As explained in [10], the most interesting case is when $\tau = O(\varepsilon)$. For $\varepsilon \ll \tau$, the limit can be obtained by first letting $\varepsilon \to 0$ and then $\tau \to 0$, giving the same result as in the continuous case described in [3]. For $\tau \ll \varepsilon$, the set will be *pinned*; i.e., the limit $D(t)$ is constant, reflecting the fact that there are a lot of local minima at the discrete level. Hence, in the following we will set $\tau = \alpha\varepsilon$ for $0 < \alpha < \infty$. It turns out that the main features are already captured by the motion of sets resembling the Wulff shapes. General shapes can be approximated by Wulff-like sets as done in [10] and a limit motion computed accordingly. Hence, in order to concentrate on the key issues, we will only consider bisectrix-square or bisectrix-hexagon like sets. For the benefit of presenting the proofs, we first define these objects carefully (see Fig. 7).

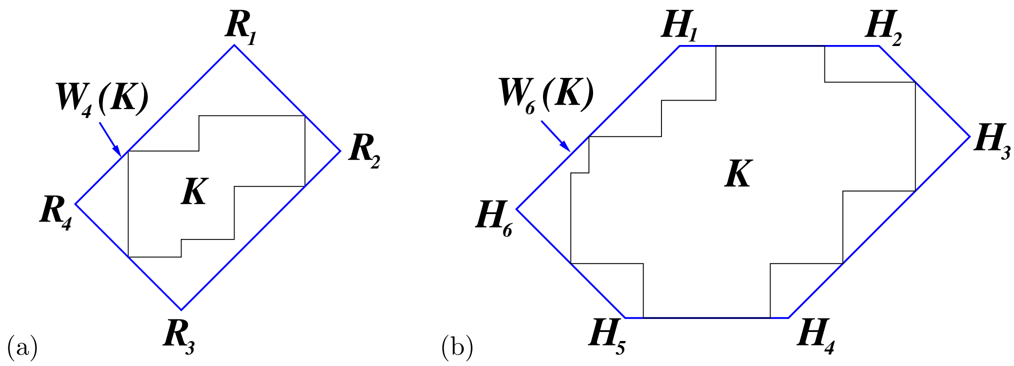

Figure 7: (a) Wulff-like rectangle and Wulff-like envelope $W_4(K)$ for ψ_1; (b) Wulff-like hexagon and Wulff-like envelope $W_6(K)$ for ψ_2.

Definition 2.7 (Wulff-like sets)**.** 1. *Let $w^\infty = e_2$. A rectangle $\mathcal{R} = R_1R_2R_3R_4$ (labelled clockwise) is called a* Wulff-like rectangle *if the vertices $R_i \in \varepsilon\mathbb{Z}^2$ (for $i = 1, 2, 3, 4$) and the sides R_1R_2, R_2R_3, R_3R_4, R_4R_1 are bisectrix segments.*

2. *Let $w^\infty = -e_1$. A hexagon $\mathcal{H} = H_1H_2H_3H_4H_5H_6$ (labelled clockwise) is called a* Wulff-like hexagon *if $H_i \in \varepsilon\mathbb{Z}^2$ (for $i = 1, 2, 4, 5$), and the segments H_1H_2 and H_4H_5 are horizontal and H_2H_3, H_3H_4, H_5H_6, H_6H_1 are bisectrix segments.*

We further let

$$\mathcal{R}_\varepsilon = \bigcup \{Q_\varepsilon \in \mathcal{Q}_\varepsilon : Q_\varepsilon \subset \mathcal{R}\}, \ \ \textit{and} \ \ \mathcal{H}_\varepsilon = \bigcup \{Q_\varepsilon \in \mathcal{Q}_\varepsilon : Q_\varepsilon \subset \mathcal{H}\}, \tag{2.27}$$

to be the union of all the squares inside $\mathcal{R}$ and $\mathcal{H}$. For convenience, we also call $\mathcal{R}_\varepsilon$ and $\mathcal{H}_\varepsilon$ a Wulff-like rectangle and hexagon, respectively.

For each $K = \bigcup_{i\in\mathcal{I}\subset\varepsilon\mathbb{Z}^2} \{Q_\varepsilon(i)\}$, a union of some collection of squares, we define the Wulff-like envelope *$W(K)$ to be the* smallest *Wulff-like rectangle and hexagon enclosing K. To be more specific, we use the notation $W_4(K)$ for the case $w^\infty = e_2$ and $W_6(K)$ for the case $w^\infty = -e_1$. See Fig. 7 for an illustration of the above definitions.*

We remark that for the definition of $\mathcal{R}$, all the vertices are required to be lattice points. In this case, there exists a unique $u \in \mathcal{S}_\varepsilon^\infty$ such that $K_u = \mathcal{R}_\varepsilon$ and all the minimizing conditions are satisfied for the slicing estimates in the vertical and horizontal directions (Lemma 2.4). However, for the definition of $\mathcal{H}$, the vertices H_3 and H_6 can be lattice points or centers of a square. We call the former as **Type I** vertex and the latter as **Type II** vertex. In either case, there is a unique $u \in \mathcal{S}_\varepsilon^\infty$ such that $K_u = \mathcal{H}_\varepsilon$ with the interfacial energy $E_\varepsilon^{(1)}(\partial_\varepsilon K_u)$ as small as possible. The structure of the **Type I** and **Type II** vertices at the discrete level will be discussed in detail in Section 3.

From now on, we will strengthen condition **(H1)** to the following:

$$c_2 > c_1 \tag{\textbf{H2}}$$

which is to ensure that $f(e_3) > f(e^3)$. For otherwise, new phases of e_3 might appear. See Section 2.4 for a more detailed explanation. With this condition, the following are our main results.

We first consider the case of crystalline motion of Wulff rectangles between e_1 and e_2 interfaces. In this case the limit motion is a motion by crystalline curvature of the e_1-set depending on a discontinuous right-hand side which is in complete analogy with the case studied in [10]. We define the *crystalline curvature* of a side of a Wulff-like rectangle with length L as

$$\kappa = \frac{2c_2}{L}. \tag{2.28}$$

This is the crystalline curvature corresponding to the continuous perimeter functional

$$\int_{\partial A} \psi_1(\nu_A) d\mathcal{H}^1,$$

where ν_A denotes the exterior normal to A, normalized by the *mobility* factor $1/\sqrt{2}$.

The metric of convergence of the K_τ^k is given by the Hausdorff distance which is defined in the following: for any $A, B \subset \mathbb{R}^2$,

$$d_{\mathcal{H}}(A,B) = \max\left\{ \sup_{y\in B\setminus A} \mathrm{Dist}(y,A), \sup_{x\in A\setminus B} \mathrm{Dist}(x,B) \right\} \tag{2.29}$$

where $\mathrm{Dist}(y,A) = \inf_{x\in A} |y-x|$ and likewise, $\mathrm{Dist}(x,B) = \inf_{y\in B} |x-y|$.

Theorem 2.8 (Crystalline motion of interfaces between e_1 and e_2 for Wulff-like rectangles)**.** *Let $D_0 \subset \mathbb{R}^2$ and $K_\tau^0 = K_{u_\tau^0}$ be Wulff-like rectangles such that $\lim_{\tau\to 0} d_{\mathcal{H}}(K_\tau^{(0)}, D_0) = 0$. Let further $\{K_\tau^k\}_{k=1,2,\ldots}$ be the sequence of sets obtained from the Euler scheme in* (2.26)*.*

Then, up to subsequence, the time-dependent set $\{K_\tau^{\lfloor \frac{t}{\tau} \rfloor}\}_{t\geq 0}$ converges in $d_{\mathcal{H}}$ to $\{D(t)\}_{t\geq 0}$ with $D(0) = D_0$, and each $D(t)$ is a Wulff-like rectangle with side lengths $\{L_i(t), i = 1,\ldots,4\}$. Each side moves with inward normal velocity $V_i(t)$ given by:

$$V_i(t) \begin{cases} = \dfrac{\sqrt{2}}{\alpha}\left\lfloor \dfrac{\alpha}{\sqrt{2}}\kappa_i(t) + \dfrac{1}{4}\right\rfloor, & \textit{if } \frac{\alpha}{\sqrt{2}}\kappa_i(t) + \frac{1}{4} \notin \mathbb{N}, \\ \\ \in \left[\kappa_i(t) - \dfrac{3\sqrt{2}}{4\alpha}, \kappa_i(t) + \dfrac{\sqrt{2}}{4\alpha}\right], & \textit{if } \frac{\alpha}{\sqrt{2}}\kappa_i(t) + \frac{1}{4} \in \mathbb{N}, \end{cases} \qquad \textit{where } \kappa_i = \frac{2c_2}{L_i(t)}. \tag{2.30}$$

See Fig. 19 for an illustration. Note that the case $\frac{\alpha}{\sqrt{2}}\kappa_i(t) + \frac{1}{4} \in \mathbb{N}$ is exceptional in the sense that the set of κ_i satisfying the condition has measure zero. As a consequence this condition is relevant only in the case when it holds for a set of non-zero measure of t. This may happen only if one of the side is pinned, and is discussed in detail in [10].

The proof of the above theorem is outlined in Section 4. An explanation of the result and the underlying velocity law is also provided at the end of Section 4. Note in particular that if we let $\alpha \to +\infty$ the law of motion tends to $V_i = \kappa_i$; i.e., motion by crystalline curvature (upon a constant mobility factor).

The formulation for the limit motion of crystalline interfaces between e_1 and $-e_1$ patterns is more complicated. We have an interesting phenomenon: that the velocity of a bisectrix side is given by a function of both its own curvatures and its bisectrix neighbour's. Hence, it is in some sense "non-local". This is due to the fact that at the level of space-time discretization, the motion can either involve only **Type I** or **Type II** vertices, or toggle between them. This is a new type of microscopic effect affecting the homogenized macroscopic velocity.

In order to describe the dynamics of the sides of $D(t)$, we first give the definition of the *crystalline curvature of each side.* The curvature κ of a horizontal side of side-length L is given by

$$\kappa = \frac{8c_2}{L}, \tag{2.31}$$

and that of a bisectrix side of side-length L is given by

$$\kappa = \frac{8(4c_2 - 2c_1)}{L}. \tag{2.32}$$

Again, this definition is related to the crystalline perimeter given by ψ_2, but takes into account mobility factors due to the anisotropy of the dissipation or mobility function.

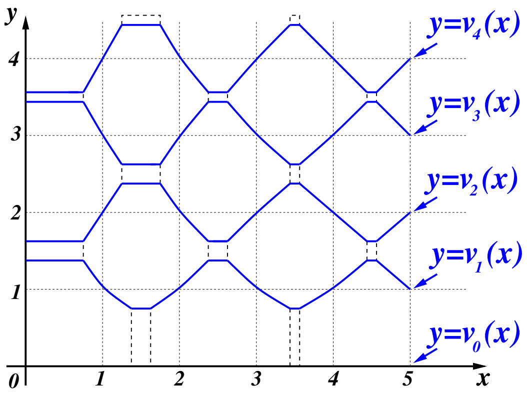

Figure 8: The curves $y = v_n(x)$ defined in (2.33) and (2.34).

Definition 2.9 (non-local law of motion)**.** *We define the function $V : [0, +\infty) \times [0, +\infty) \to \mathbb{N}$ as follows.*

1. *Let $n \geq 1$ be odd. For $m \geq 0$,*

$$v_n(x) = \begin{cases} \min\left\{\dfrac{nx}{m}, n\left(1 + \dfrac{c_1}{2(c_2 - c_1)}\right), \dfrac{nx}{2x - (m+1)}\right\}, & \text{if } m \leq x \leq m+1, \ m \text{ even}, \\ \max\left\{\dfrac{nx}{2x - m}, n\left(1 - \dfrac{c_1}{2c_2}\right), \dfrac{nx}{m+1}\right\}, & \text{if } m \leq x \leq m+1, \ m \text{ odd}. \end{cases} \tag{2.33}$$

2. *$v_0(x) \equiv 0$ and for $m \geq 0$, n even and positive,*

$$v_n(x) = \begin{cases} \max\left\{\dfrac{nx}{2x - m}, n\left(1 - \dfrac{c_1}{2c_2}\right), \dfrac{nx}{m+1}\right\}, & \text{if } m \leq x \leq m+1, \ m \text{ even}, \\ \min\left\{\dfrac{nx}{m}, n\left(1 + \dfrac{c_1}{2(c_2 - c_1)}\right), \dfrac{nx}{2x - (m+1)}\right\}, & \text{if } m \leq x \leq m+1, \ m \text{ odd}. \end{cases} \tag{2.34}$$

3. *For $n \in \mathbb{N}$, let $V(x, y) = n$ for $v_n(x) < y \leq v_{n+1}(x)$.*

See Fig. 8 for an illustration of (2.33) and (2.34).

Theorem 2.10 (Crystalline motion of interfaces between e_1 and $-e_1$ for Wulff-like hexagons)**.** *Let $D_0 \subset \mathbb{R}^2$ and $K_\tau^0 = K_{u_\tau^0}$ be Wulff-like hexagons such that $\lim_{\tau\to 0} d_{\mathcal{H}}(K_\tau^{(0)}, D_0) = 0$.*

Then, up to subsequence, the time-dependent set $\{K_\tau^{\lfloor \frac{t}{\tau} \rfloor}\}_{t\geq 0}$ converges in $d_{\mathcal{H}}$ to $\{D(t)\}_{t\geq 0}$ with $D(0) = D_0$, and each $D(t)$ is a Wulff-like hexagon with side lengths $\{L_i(t), i = 1, \ldots 6\}$.

Let κ_i denote the crystalline curvature of the side L_i. Then the horizontal sides $i = 1, 4$ move with inward normal velocities V_i given by:

$$V_i \begin{cases} = \dfrac{1}{\alpha} \lfloor \alpha\kappa_i \rfloor, & \text{if } \alpha\kappa_i \notin \mathbb{N} \\ \\ \in \left[\dfrac{1}{\alpha}(\alpha\kappa_i - 1), \kappa_i\right], & \text{if } \alpha\kappa_i \in \mathbb{N}. \end{cases} \tag{2.35}$$

The bisectrix sides $i = 2, 3, 5, 6$ move inwards with velocity

$$V_2(\kappa_2, \kappa_3) = \frac{1}{\alpha\sqrt{2}} V(\alpha\kappa_3, \alpha\kappa_2), \quad V_3(\kappa_2, \kappa_3) = \frac{1}{\alpha\sqrt{2}} V(\alpha\kappa_2, \alpha\kappa_3), \tag{2.36}$$

$$V_5(\kappa_5, \kappa_6) = \frac{1}{\alpha\sqrt{2}} V(\alpha\kappa_5, \alpha\kappa_6), \quad V_6(\kappa_5, \kappa_6) = \frac{1}{\alpha\sqrt{2}} V(\alpha\kappa_6, \alpha\kappa_5) \tag{2.37}$$

at all times such that $(\alpha\kappa_2, \alpha\kappa_3), (\alpha\kappa_5, \alpha\kappa_6) \notin X$, where

$$X = \{(x, y) \in [0, +\infty) \times [0, +\infty) : x = v_n(y) \text{ or } y = v_n(x),\ n \in \mathbb{N}\}.$$

As mentioned above, the form of the velocities V_i for the bisectrix sides is due to the possibility of Type I and Type II vertices. The curves $y = v_n(x)$ and $x = v_n(y)$ partition the plane into regions such that if the ordered pairs of scaled curvatures $(\alpha\kappa_2, \alpha\kappa_3)$ and $(\alpha\kappa_5, \alpha\kappa_6)$ fall into one of this regions, then during the evolution, the vertices H_3 and H_6, which are the intersection between the two consecutive bisectrix sides, will either maintain the same type, or alternate between them. In Section 5.2, we describe those regions and derive the velocity law. In that perspective, we also find it instructive to express the motion laws V_2, V_3 (2.36) (and similarly for V_5, V_6 (2.37)) in the following fashion:

$$V_2 = \frac{1}{\alpha\sqrt{2}} \left(\lfloor \alpha\kappa_2 \rfloor + p\right), \text{ and } V_3 = \frac{1}{\alpha\sqrt{2}} \left(\lfloor \alpha\kappa_3 \rfloor + q\right), \text{ for } \alpha\kappa_2, \alpha\kappa_3 \notin \mathbb{N}. \tag{2.38}$$

where $p = p(\alpha\kappa_2, \alpha\kappa_3), q = q(\alpha\kappa_2, \alpha\kappa_3) \in \{-1, 0, 1\}$ are functions of *both* κ_2 and κ_3. The precise forms of p and q are given in terms of the sets $\mathbf{V}(m, n)$ and $\mathbf{D}(m, n)$ which are defined in (5.38) and (5.52) and illustrated in Fig. 26 and 27 for $m, n \in \mathbb{N}$. The explicit expressions for p and q are given in (5.46)–(5.51). As a further illustration, the inverse image of the velocity functions V_2 and V_3 are depicted in Fig. 9, which are a consequence of Fig. 28 and 29.

The above theorem will be proved in Section 5, in particular Section 5.2.

Remark 2.11.

1. The different cases in the above formulation are described by open sets $\alpha\kappa_i \notin \mathbb{N}$ for horizontal sides, or $(\alpha\kappa_i, \alpha\kappa_{i+1}) \notin X$ for pairs of bisectrix sides. For simplicity, we do not dwell into the details about the boundary cases, which seem more complex than those in [10], but we refer to the end of Section 4 for some discussion.

2. In the case $\alpha \to +\infty$ we recover the limit laws of motion $V_i = \kappa_i$ for horizontal sides and $V_i = \frac{1}{\sqrt{2}}\kappa_i$ for bisectrix sides, which coincide with the ones obtained in [3]. Note that the limit motions of all V_i are decoupled.

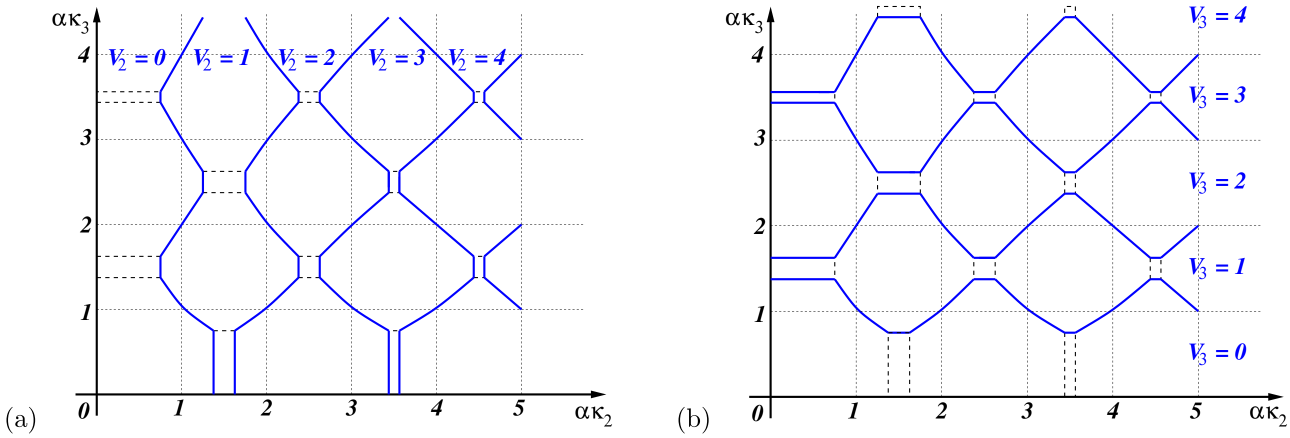

Figure 9: Partitioning of the $\kappa_2\kappa_3$-plane into: (a) $\left\{V_2^{-1}\{m\}\right\}_{m\geq 0}$, and (b) $\left\{V_3^{-1}\{n\}\right\}_{n\geq 0}$.

2.4 Remarks about the conditions on c_1, c_2

Hypothesis (H1): $2c_2 > c_1$**.** This condition ensures that the ground state patterns are $\pm e_1$ and $\pm e_2$. Otherwise, it can be shown as in [1] that upon suitable affine change of variable, the ground state is given by e_3 and the analysis is equivalent to that of the ferromagnetic case. Hence, the Wulff shape is a square and after a change of parameters, the analysis of [10] applies.

Hypothesis (H2): $c_2 > c_1$**.** This is a technical simplification to prevent the appearance of new phase such as e_3. Under this assumption, the energy of any non-ground state patterns $(e^3, \pm e_3, \pm e_8)$ is at least $2c_2$. Hence, we can reduce the computation of the energy of the interfacial region to appropriate bond counting strategy. Otherwise, we need to make use of some isoperimetric inequality to investigate the competition between interfacial and bulk energy terms.

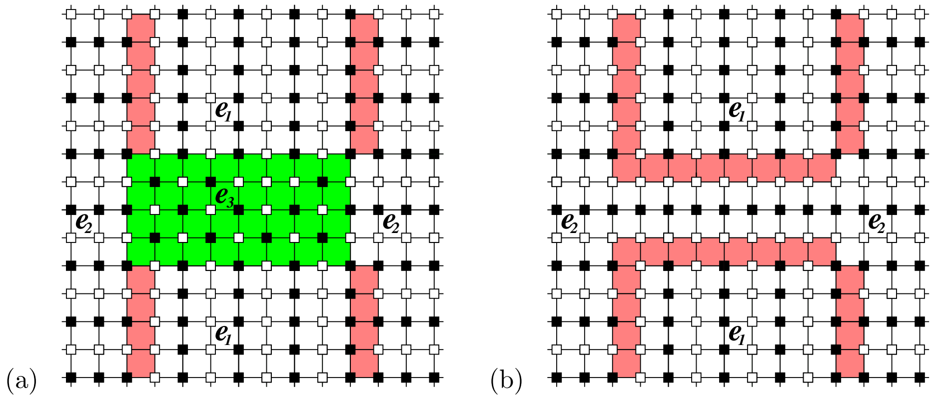

Figure 10: With the introduction of some e_3-phase inside e_1- and e_2-phases (in (a)), the interfacial energy can be lower than without the e_3-phase (in (b)) as the energy of e_3 can be very low.

As an illustration of the possibility of the appearance of e_3 if this hypothesis is not satisfied, suppose we have otherwise that

$$c_1 > c_2 \approx \frac{1}{2}c_1.$$

In this case the energy of e_3, given by $4c_2 - 2c_1$, is very low, or close to zero. So in principle, the appearance of e_3 will not cause any extra interfacial energy. In essence e_3 can actually be a "new ground sate". In fact, the interfacial energy of the overall pattern might actually decrease. For example, consider the case of e_1-crystal embedded in e_2 as in Figure 10. Note that there is no extra interfacial energy between e_1, e_3, and e_2, e_3. The actual advantage for the introduction of the extra e_3 phase will depend on the competition between the interfacial and bulk energies which in turn depends on some isoperimetric inequality. Hence, to keep our analysis within reasonable complexity, we will eliminate such a complication by means of condition (**H2**).

2.5 Some Additional Notation

Here we introduce some notation to facilitate our proof.

1. Even though we are only concerned with functions w from $\mathcal{W}$, we find it convenient to also consider functions from $\widetilde{\mathcal{W}}$ which are not necessarily realized by a spin function $u \in \mathcal{S}_\varepsilon$. The following notation and definitions still make sense: for $\widetilde{w} \in \widetilde{\mathcal{W}},\ u \in \mathcal{S}_\varepsilon^\infty$,

$$E_\varepsilon^{(1)}(\widetilde{w}) = \varepsilon \sum_{i \in \varepsilon\mathbb{Z}^2} f(\widetilde{w}_i), \tag{2.39}$$

$$\mathcal{F}_{\varepsilon,\tau}(\widetilde{w}, u) = E_\varepsilon^{(1)}(\widetilde{w}) + \frac{\varepsilon^2}{\tau} \sum_{\{i \in \varepsilon\mathbb{Z}^2 :\ \widetilde{w}_i \neq w(u)_i\}} \mathrm{Dist}_\varepsilon^1(Q_\varepsilon(i), \partial_\varepsilon K_u). \tag{2.40}$$

2. For all $u \in \mathcal{S}_\varepsilon$, $\widetilde{w} \in \widetilde{\mathcal{W}}$ and $A = \bigcup \{Q_\varepsilon\}$ the union of a collection of squares from $\mathcal{Q}_\varepsilon$,

$$E_\varepsilon^{(1)}(u, A) = \varepsilon \sum_{Q_\varepsilon(i) \subseteq A} f(w(u)_i), \tag{2.41}$$

$$E_\varepsilon^{(1)}(\widetilde{w}, A) = \varepsilon \sum_{Q_\varepsilon(i) \subseteq A} f(\widetilde{w}(i)). \tag{2.42}$$

3. Let $A = \bigcup \{Q_\varepsilon(i) : i \in \mathcal{I}\}$ be the union of a collection of some squares from $\mathcal{Q}_\varepsilon$:

(a) ∂A denotes the topological boundary of A. Note that ∂A is a union of horizontal and vertical segments.

(b) $\partial_\varepsilon^1 A$ denotes those squares $Q_\varepsilon(i) \nsubseteq A$ but whose center $q_\varepsilon(i)$ is at an L^1-distance ε from the set of centers of A, $\{q_\varepsilon(i) : i \in \mathcal{I}\}$.

4. For any set A, $\#\{A\}$ denotes the number of elements in A. For the sake of simplicity, if $A = \bigcup \{Q_\varepsilon\}$ is the union of a collection of squares, $\#\{A\}$ means the number of squares inside A.

3 Discrete Wulff Shapes

Here we investigate at the discrete level the Wulff shapes for ψ_1 and ψ_2. In order to formulate statements that are useful for our analysis, we will characterize the *Wulff-like envelopes* of a given e_1-crystal as the shape of a set containing the given crystal with the *smallest interfacial energy* while enclosing *as many squares as possible*. Precise statements will be given in Propositions 3.1 and 3.2.

For e_1 inside e_2, the structure of the Wulff shape is simple, as indicated in Figure 6(a).

For e_1 inside $-e_1$, Figure 6(b) shows a *perfect* (Type I) hexagonal Wulff shape. We call it 'perfect' as everywhere it locally achieves the minimum energy in the slicing estimates (recall Lemma 2.4). Note that in this case the bisectrix sides intersect at a lattice point. However, a different energy minimizing pattern (Type II) can arise if the bisectrix sides intersect at the center of a square. We illustrate this with the example shown in Figure 11.

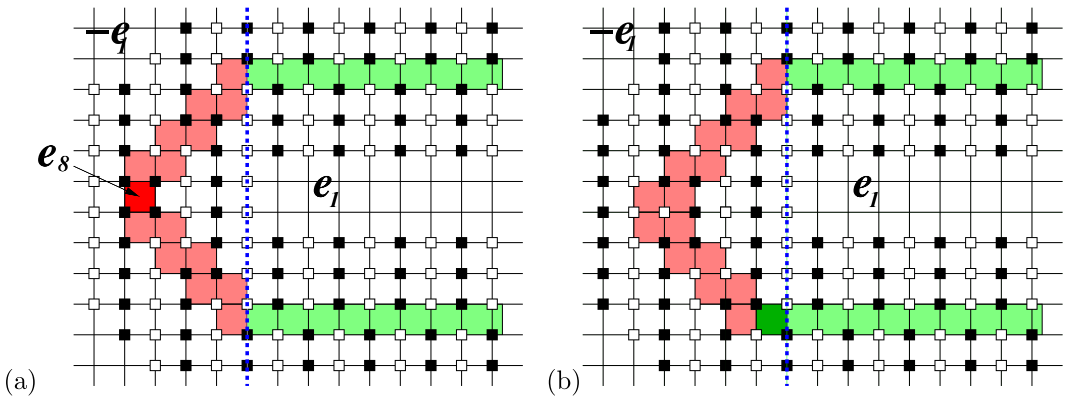

Figure 11: Comparison of the interfacial energies for discrete hexagonal-like Wulff shapes for ψ_2 with different type of vertices. (Only the energies to the left of the dotted vertical lines are compared.) The result is that even with the presence of the *high energy* pattern e_8 (**Type II** vertex), the interfacial structure in (a) has a *smaller energy* than the structure in (b) (with a **Type I** vertex).

For the pattern in Figure 11(a), the energy of the interfacial region (to the left of the vertical dotted line) is:

$$2 \times f(e^3) + 6 \times 2f(e^3) + f(e_8). \tag{3.1}$$

Note the appearance of one e_8 defect that seemingly costs a lot of energy.

On the other hand, if we move the lower bisectrix side *outward* by one square, the e_8 defect can be eliminated (see Fig. 11(b)). In this case, the energy of the interfacial region is:

$$2 \times f(e^3) + 7 \times 2f(e^3) + f(e_3). \tag{3.2}$$

Note the appearance of an additional e_3. Now we compare the energy of both patterns:

$$\begin{aligned}
& \text{Energy(Figure 11(b))} - \text{Energy(Figure 11(a))} \\
= \quad & \varepsilon\Big[2f(e^3) + 14f(e^3) + f(e_3)\Big] - \varepsilon\Big[2f(e^3) + 12f(e^3) + f(e_8)\Big] \\
= \quad & \varepsilon\Big[2f(e^3) + f(e_3) - f(e^8)\Big] \\
= \quad & \varepsilon\Big[2(2c_2) + (4c_2 - 2c_1) - (4c_2 + 2c_1)\Big] \\
= \quad & \varepsilon\Big[4c_2 - 4c_1\Big] > 0 \quad (\text{as } c_2 > c_1 \text{ by } (\mathbf{H2})).
\end{aligned}$$

Hence, moving outward can cost more energy, leading to a competition between the interfacial energy and the incremental bulk term in $\mathcal{F}_{\varepsilon,\tau}$. The effect of this competition on the dynamical equation will be analyzed carefully in Section 5.2.

We will formulate and summarize the above considerations about Wulff shapes in the next two sections. The results are interesting in their own right and will also be useful for later analysis.

Before presenting the proofs, we first recall the Definition 2.7 of Wulff-like sets (rectangle, hexagon) $\mathcal{R}$, $\mathcal{R}_\varepsilon$, $\mathcal{H}$, $\mathcal{H}_\varepsilon$, and the Wulff-like envelopes $W_4(\Omega)$, $W_6(\Omega)$ for a subset Ω of $\mathbb{R}^2$. For each $\mathcal{R}$, there is a unique $v \in \mathcal{S}_\varepsilon^\infty$ such that $K_v = \mathcal{R}_\varepsilon$ and $\partial_\varepsilon K_v$ everywhere satisfies the minimizing slicing estimates described in Lemma 2.4. See Fig. 6(a). For each $\mathcal{H}$, if H_3 and H_6 are lattice points; i.e., they are Type I vertices, there is again a unique $v \in \mathcal{S}_\varepsilon^\infty$ such that $K_v = \mathcal{H}_\varepsilon$ and $\partial_\varepsilon K_v$ everywhere satisfies the minimizing slicing estimates described in Lemma 2.4. See Fig. 6(b). However, if H_3 or H_6 is the center of some square; i.e., they are Type

II vertices, then we will choose the v as illustrated in Figure 11(a) so that there is a defect of e_8 appearing at the vertex. In all of the above, for simplicity, the corresponding $\partial_\varepsilon K_v$ will be denoted by $\partial_\varepsilon \mathcal{R}_\varepsilon$ and $\partial_\varepsilon \mathcal{H}_\varepsilon$.

3.1 Discrete Wulff Shape for e_1-Phase Inside e_2-Phase

In this section, we identify the shape enclosing a given e_1-crystal which has the smallest energy value for ψ_1 and yet contains as many squares as possible. The answer is given by the smallest Wulff-like rectangle containing the crystal.

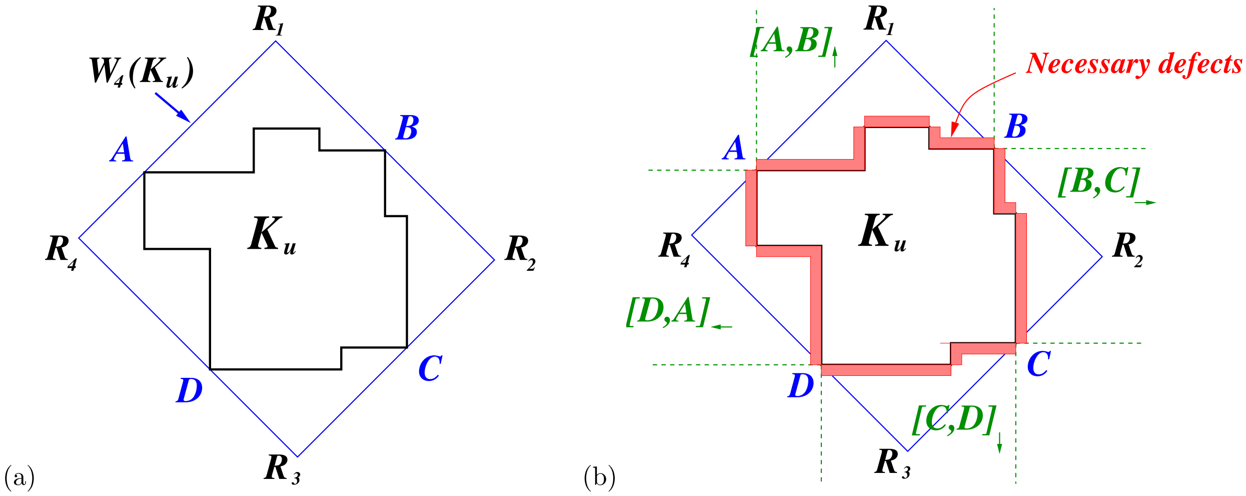

Figure 12: (a) Wulff-like rectangular envelope $W_4(K_u)$ enclosing K_u. (b) Computing the lower bound of $E^{(1)}_\varepsilon(K_u)$ by means of projection and slicing estimates.

Proposition 3.1. *Let $w^\infty = e_2$, $u \in \mathcal{S}^\infty_\varepsilon$. Suppose $K_u = \bigcup\{Q_\varepsilon(i) : w(u)_i = e_1\}$ be connected. Then*

$$E^{(1)}_\varepsilon(u) \geq \min\left\{E^{(1)}_\varepsilon(v) : \ K_u \subseteq K_v \text{ and } K_v \text{ is a Wulff-like rectangle.}\right\} \tag{3.3}$$

The minimum of the above right-hand side is uniquely attained at the Wulff-like envelope of K_u: $W_4(K_u)$. (See Fig. 12.)

Proof. Let $\mathcal{R} = R_1R_2R_3R_4 \subseteq \mathbb{R}^2$ be the smallest bisectrix-rectangle containing K_u. Then ∂K_u touches $\partial\mathcal{R}$ at some points A, B, C, and $D \in \varepsilon\mathbb{Z}^2$ on R_4R_1, R_1R_2, R_2R_3 and R_3R_4 (see Fig. 12). (Note that there might be multiple such points. Any one suffices for our argument.)

Next we partition $\mathbb{R}^2\backslash K_u$ into four regions so that we can employ vertical and horizontal slicings. More precisely, we first divide the boundary curve ∂K_u (traced clockwise) into four sets: $\partial K_u\big|_{[A,B]}$, $\partial K_u\big|_{[B,C]}$, $\partial K_u\big|_{[C,D]}$, and $\partial K_u\big|_{[D,A]}$. Then let:

$$[A,B]_\uparrow \text{ be the region bounded by } \{(x_A, y) : y > y_A\} \cup \partial K_u\big|_{[A,B]} \cup \{(x_B, y) : y > y_B\}\,; \tag{3.4}$$

$$[B,C]_\rightarrow \text{ be the region bounded by } \{(x, y_B) : x_B < x\} \cup \partial K_u\big|_{[B,C]} \cup \{(x, y_C) : x_C < x\}\,; \tag{3.5}$$

$$[C,D]_\downarrow \text{ be the region bounded by } \{(x_C, y) : y < y_C\} \cup \partial K_u\big|_{[C,D]} \cup \{(x_D, y) : y < y_D\}\,; \tag{3.6}$$

$$[D,A]_{\leftarrow} \text{ be the region bounded by } \left\{(x,y_D) : x < x_D\right\} \cup \partial K_u\big|_{[D,A]} \cup \left\{(x,y_A) : x < x_A\right\}. \tag{3.7}$$

The above are essentially the projections of ∂K_u toward the upwards, right, downwards and left directions. By the slicing estimates in Lemma 2.4 we have

$$\begin{aligned}
E^{(1)}_\varepsilon\Big(\partial_\varepsilon K_u, [A,B]_\uparrow\Big) &\geq f(e^3)(x_B - x_A) = (2c_2)(x_B - x_A),\\
E^{(1)}_\varepsilon\Big(\partial_\varepsilon K_u, [B,C]_\rightarrow\Big) &\geq f(e^3)(y_B - y_C) = (2c_2)(y_B - y_C),\\
E^{(1)}_\varepsilon\Big(\partial_\varepsilon K_u, [C,D]_\downarrow\Big) &\geq f(e^3)(x_C - x_D) = (2c_2)(x_C - x_D),\\
E^{(1)}_\varepsilon\Big(\partial_\varepsilon K_u, [D,A]_\leftarrow\Big) &\geq f(e^3)(y_A - y_D) = (2c_2)(y_A - y_D).
\end{aligned}$$

Now suppose all the vertices of $\mathcal{R}$ are lattice points. Then $\mathcal{R}$ is a Wulff-like rectangle. We claim that

$$E^{(1)}_\varepsilon(\partial_\varepsilon K_u) \geq E^{(1)}_\varepsilon(\partial_\varepsilon \mathcal{R}_\varepsilon). \tag{3.8}$$

This is simply due to the fact that (see Fig. 12(b))

$$\begin{aligned}
E^{(1)}_\varepsilon\Big(\partial_\varepsilon \mathcal{R}_\varepsilon, [A,B]_\uparrow\Big) &= (2c_2)(x_B - x_A),\\
E^{(1)}_\varepsilon\Big(\partial_\varepsilon \mathcal{R}_\varepsilon, [B,C]_\rightarrow\Big) &= (2c_2)(y_B - y_C),\\
E^{(1)}_\varepsilon\Big(\partial_\varepsilon \mathcal{R}_\varepsilon, [C,D]_\downarrow\Big) &= (2c_2)(x_C - x_D),\\
E^{(1)}_\varepsilon\Big(\partial_\varepsilon \mathcal{R}_\varepsilon, [D,A]_\leftarrow\Big) &= (2c_2)(y_A - y_D).
\end{aligned}$$

Next suppose some of the vertices of $\mathcal{R}$ are at the center of a square, then we can find an enlarged Wulff-like rectangle $\widetilde{\mathcal{R}}$ which contains $\mathcal{R}$ and the following lower bound is satisfied:

$$E^{(1)}_\varepsilon(\partial_\varepsilon K_u) \geq E^{(1)}_\varepsilon(\partial_\varepsilon \widetilde{R}_\varepsilon). \tag{3.9}$$

To prove the above, we consider the parity of the points A, B, C and D in relation to the pattern e_2 (recall Definitions 2.2 and 2.3). If any of the points A, B, C and D has odd parity, then we will shift the point *outward* horizontal by one lattice point. For concreteness, if A (B, C or D) has odd parity, then we shift it to $\widetilde{A} = (x_A - \varepsilon, y_A)$ ($\widetilde{B} = (x_B + \varepsilon, y_C)$, $\widetilde{C} = (x_C + \varepsilon, y_C)$, or $\widetilde{D} = (x_D - \varepsilon, y_D)$). Then the bisectrix-rectangle $\widetilde{\mathcal{R}}$ constructed by the new points $\widetilde{A}, \widetilde{B}, \widetilde{C}, \widetilde{D}$ will contain $\mathcal{R}$ and its vertices will all lie on lattice points. Hence, $\widetilde{\mathcal{R}}_\varepsilon$ is a Wulff-like rectangle. As before we can construct a spin function $v_2 \in \mathcal{S}_\varepsilon$ such that $\widetilde{\mathcal{R}}_\varepsilon = K_{v_2}$.

The reason for (3.9) is that whenever a touching point has odd parity, there must be an extra defect appearing in $\partial_\varepsilon K_u$. For example, if A has odd parity, then $w(Q_\varepsilon(\widetilde{A})) \neq \pm e_1, \pm e_2$; i.e., it must be a defect (recall Definition 2.2 of the tessellations $[\pm e_1], [\pm e_2]$). By our assumption $c_2 > c_1$, its energy is at least that of e^3 so that (3.9) holds. (See Fig. 13.) □

3.2 Discrete Wulff Shape for e_1 Inside $-e_1$

Here we similarly identify the set enclosing a given e_1-crystal with the property that it has the minimum interfacial energy ψ_2 and yet contains as many squares as possible. The answer is again given by the Wulff-like envelope (hexagon) containing the crystal. However, this case is complicated by the following two facts:

(i) for interfaces along the horizontal direction, the minimum energy cost is $f(e_3) = 4c_2 - 2c_1$ while for interfaces along the bisectic direction, the minimum energy cost is $2 \times f(e^3) = 2(2c_2) = 4c_2$;

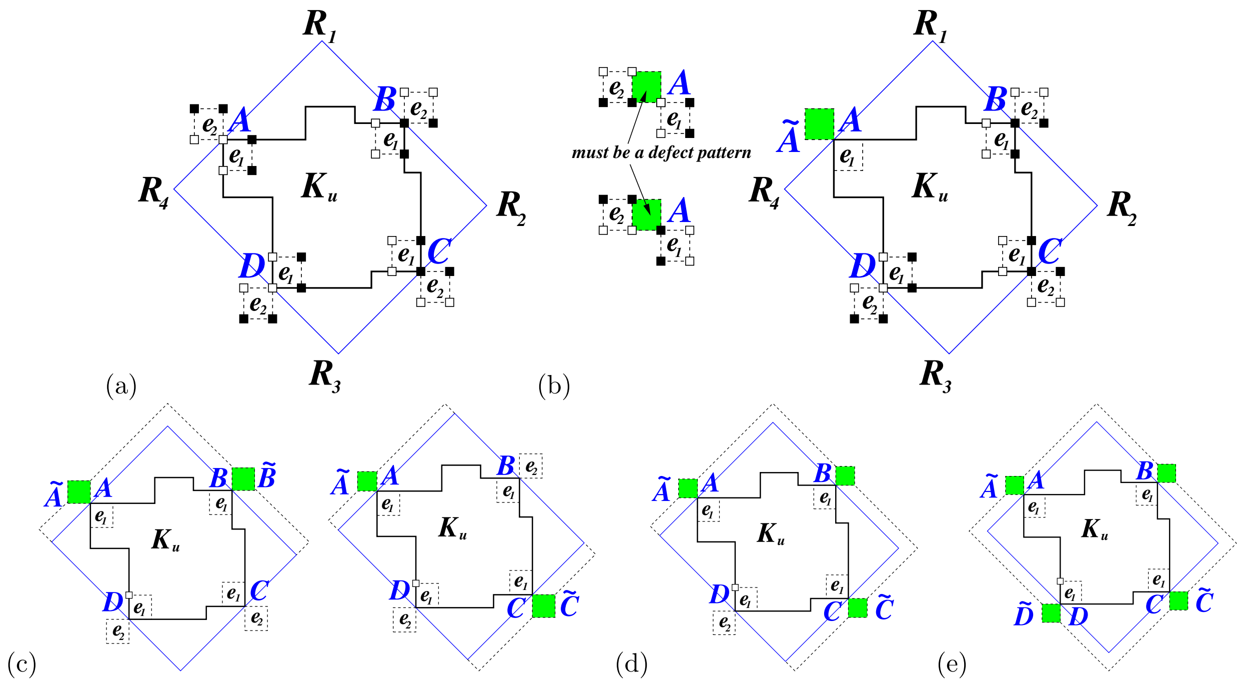

Figure 13: Wulff-like rectangle envelope enclosing K_u with: (a) all touching points having the right parity; (b) one touching point having the wrong parity; (c) two touching points having the wrong parity; (d) three touching points having the wrong parity; (e) all four touching points having the wrong parity.

(ii) for a Wulff-like hexagon $\mathcal{H} = H_1H_2H_3H_4H_5H_6$, each of the vertices H_3 and H_6 can be of Type I if it is at a lattice point, or Type II if it is at the center of a lattice point (see Fig. 11).

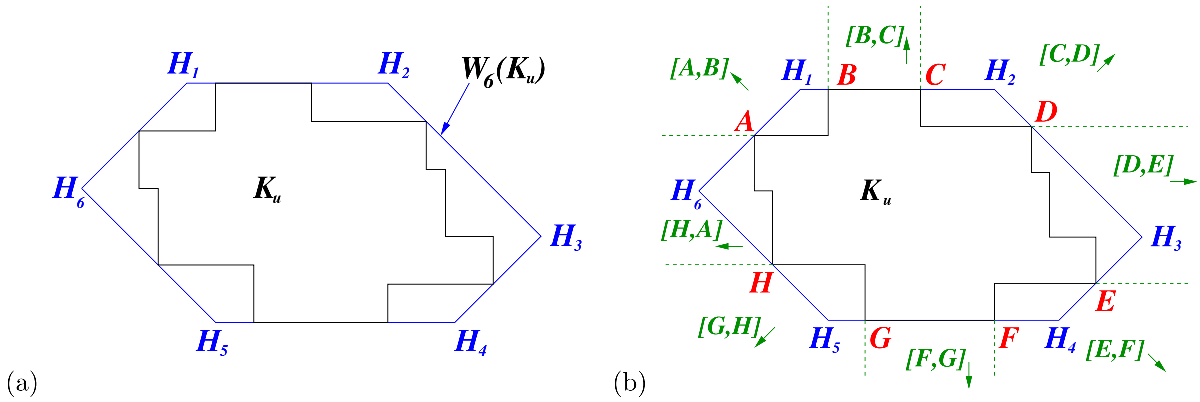

Figure 14: (a) Wulff-like hexagonal envelope $W_6(K_u)$ enclosing K_u; (b) Partitioning of $\mathbb{R}^2\backslash K_u$ into $[A,B]_{\nwarrow}$, $[B,C]_{\uparrow}$, $[C,D]_{\nearrow}$, $[D,E]_{\rightarrow}$, $[E,F]_{\searrow}$, $[F,G]_{\downarrow}$, $[G,H]_{\swarrow}$, and $[H,A]_{\leftarrow}$.

Now we present the following result.

Proposition 3.2. *Let $w^\infty = -e_1$, $u \in \mathcal{S}_\varepsilon^\infty$. Suppose $K_u = \bigcup\{Q_\varepsilon(i) : w(u)_i = e_1\}$ be connected. Then*

$$E_\varepsilon^{(1)}(u) \geq \min\left\{E_\varepsilon^{(1)}(v) : \ K_u \subseteq K_v \ \textit{and} \ K_v \ \textit{is a Wulff-like hexagon.}\right\} \tag{3.10}$$

The minimum of the above right-hand side is uniquely attained at the Wulff-like envelope of K_u: $W_6(K_u)$. The minimizer can have both Type I or Type II vertices (see Fig. 14(a)*).*

Proof. Let $\mathcal{H} = H_1H_2H_3H_4H_5H_6$ be the Wulff-like envelope $W_6(K_u)$ such that $\partial\mathcal{H}$ and ∂K_u touch at points A, B, C, D, E, F, G, H on H_6H_1, H_1H_2, H_2H_3, H_3H_4, H_4H_5 and H_5H_6, respectively (see Fig. 14(b)). We claim that

$$E_\varepsilon^{(1)}(\partial_\varepsilon K_u) \geq E_\varepsilon^{(1)}(\partial_\varepsilon \mathcal{H}_\varepsilon). \tag{3.11}$$

The above holds regardless whether H_3 or H_6 are Type I or Type II vertices.

First, similarly to (3.4)–(3.7), we define $[B,C]_\uparrow$, $[G,F]_\downarrow$, $[D,E]_\rightarrow$, $[A,H]_\leftarrow$ which are the upwards, downwards, right and left projections of ∂K_u. By one-dimensional slicing argument (Lemma 2.4), we conclude that:

$$\begin{aligned}
E_\varepsilon^{(1)}\left(\partial_\varepsilon K_u, [B,C]_\uparrow\right) &\geq f(e_3)(x_C - x_B) = (4c_2 - 2c_1)(x_C - x_B); && (3.12)\\
E_\varepsilon^{(1)}\left(\partial_\varepsilon K_u, [G,F]_\downarrow\right) &\geq f(e_3)(x_F - x_G) = (4c_2 - 2c_1)(x_F - x_G); && (3.13)\\
E_\varepsilon^{(1)}\left(\partial_\varepsilon K_u, [D,E]_\rightarrow\right) &\geq 2f(e^3)(y_D - y_E) = 4c_2(y_D - y_E); && (3.14)\\
E_\varepsilon^{(1)}\left(\partial_\varepsilon K_u, [A,H]_\leftarrow\right) &\geq 2f(e^3)(y_A - y_H) = 4c_2(y_A - y_H). && (3.15)
\end{aligned}$$

Second, in order to analyze the squares in $\partial_\varepsilon K_u$ between $[A,B]$, we define $[A,B]_\nwarrow$ to be the region bounded by the the following curves:

$$\{(x, y_A) : x \leq x_A\} \cup \partial K_u\big|_{[A,B]} \cup \{(x_B, y) : y \geq y_B\}.$$

where $\partial K_u\big|_{[A,B]}$ is the portion of ∂K_u traced from A to B in the clockwise manner. We claim that:

$$E_\varepsilon^{(1)}(\partial_\varepsilon K_u, [A,B]_\nwarrow) \geq f(e_3)(x_B - x_{H_1}) + 2f(e^3)(y_{H_1} - y_A) + \varepsilon f(e^3). \tag{3.16}$$

The formula above comes from the pattern for the Wulff interface joining A and B. Analogous claims hold for the remaining portions of $\partial_\varepsilon K_u$: $(\partial_\varepsilon K_u, [C,D]_\nearrow)$, $(\partial_\varepsilon K_u, [E,F]_\searrow)$, and $(\partial_\varepsilon K_u, [G,H]_\swarrow)$.

To prepare for the proof of (3.16), we first define the *exterior phase L_u of the crystal K_u*. Let $O_u = \bigcup\{Q(i) : w(u)_i = -e_1\}$. Since $u \in \mathcal{S}_\varepsilon^\infty$, we have $w(u)_i = w^\infty$ $(= -e_1)$ outside some bounded subset of $\mathbb{R}^2$. Hence, we can define L_u to be the (unique) unbounded connected component of O_u. Without loss of generality, we can assume that $\mathbb{R}^2\backslash L_u$ is connected which automatically contains K_u. Suppose otherwise, on those "islands" (i.e., connected components of $\mathbb{R}^2\backslash L_u$) disjoint from K_u, we can simply replace the pattern by $-e_1$. This procedure will not increase the surface energy $E_\varepsilon^{(1)}(u)$. Next, we set $\alpha = \partial_\varepsilon^1 K_u$ and $\beta = \partial_\varepsilon^1 L_u$. These are necessarily defect patterns and hence by (H2) their energy is at least $f(e^3)\varepsilon = 2c_2\varepsilon$ for each square.

We have the following two cases:

Case I. $\alpha \cap \beta = \emptyset$ (Figure 15(a)). Then we have

$$\begin{aligned}
E_\varepsilon^{(1)}(\partial_\varepsilon K_u, \alpha) + E_\varepsilon^{(1)}(\partial_\varepsilon K_u, \beta) &= \varepsilon f(e^3)\#\{\alpha\} + \varepsilon f(e^3)\#\{\beta\}\\
&\geq 2f(e^3)(x_B - x_A) \quad \text{(by vertical slicing)}\\
&\geq f(e_3)(x_B - x_{H_1}) + 2f(e^3)(y_{H_1} - y_A). && (3.17)
\end{aligned}$$

In the above, we have used the facts that $2f(e^3) > f(e_3)$ and

$$x_B - x_A = x_B - x_{H_1} + (x_{H_1} - x_A), \quad \text{and} \quad y_B - y_A = y_{H_1} - y_A = x_{H_1} - x_A. \tag{3.18}$$

Case II. $\alpha \cap \beta \neq \emptyset$ (Figure 15(b)). Let Q_ε be a square from $\alpha \cap \beta$. Then either:

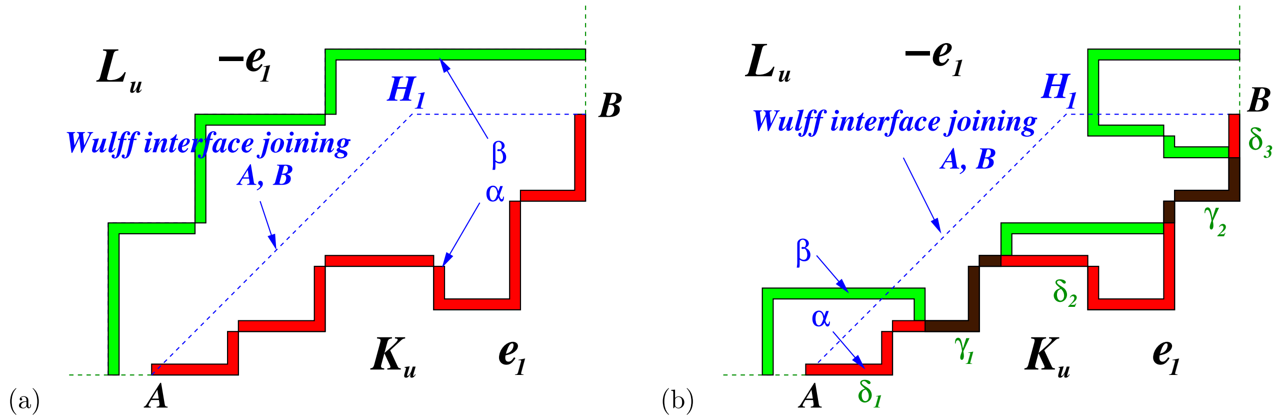

Figure 15: Estimating the interfacial energies of $\alpha = \partial_\varepsilon K_u$ and $\beta = \partial_\varepsilon L$ in the region $[A, B]_\nwarrow$: (a) $\alpha \cap \beta = \emptyset$; (b) $\alpha \cap \beta \neq \emptyset$;

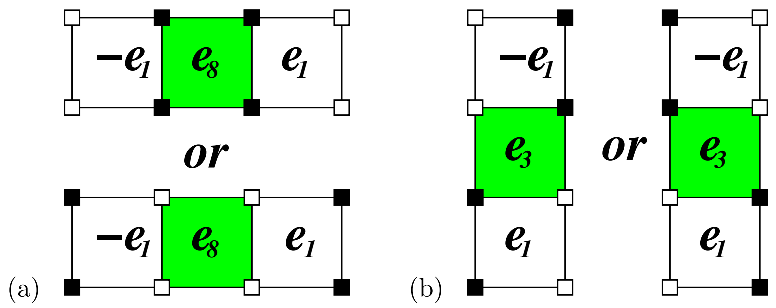

Figure 16: (a) a horizontal square Q_ε, and (b) a vertical square Q_ε.

(i) the square Q_ε is *vertical* in the sense that its nearest left and right neighbors are e_1 and $-e_1$ or $-e_1$ and e_1 (see Fig. 16(a)). In this case, we have $E_\varepsilon^{(1)}(\partial_\varepsilon K_u, Q_\varepsilon) = \varepsilon f(e_8)$.

(ii) the square Q_ε is *horizontal* in the sense that its nearest upper and lower neighbors are e_1 and $-e_1$ or $-e_1$ and e_1 (see Fig. 16(b)). In this case, we have $E_\varepsilon^{(1)}(\partial_\varepsilon K_u, Q_\varepsilon) = \varepsilon f(e_3)$.

Now consider the following partitions of α and β into their connected components:

$$\alpha = \alpha \cup (\alpha \backslash \beta) = (\gamma_1 \cup \gamma_2 \cdots) \cup (\delta_1^\alpha \cup \delta_2^\alpha \cdots) \tag{3.19}$$

$$\beta = \beta \cup (\beta \backslash \alpha) = (\gamma_1 \cup \gamma_2 \cdots) \cup (\delta_1^\beta \cup \delta_2^\beta \cdots) \tag{3.20}$$

where $\gamma_i \subseteq \alpha \cap \beta$ and γ_i is either horizontal or vertical in the sense that it consists of only horizontal or vertical arrays of squares; $\delta_j^\alpha \subseteq \alpha \backslash \beta$, and $\delta_j^\beta \subseteq \beta \backslash \alpha$. Note that $\delta_j^\alpha \cap \delta_j^\beta = \emptyset$. Then

$$E_\varepsilon^{(1)}(\partial_\varepsilon K_u, \gamma_i) = \begin{cases} \varepsilon f(e_3)\#\{\gamma_i\}, & \text{if } \gamma_i \text{ is horizontal} \\ \varepsilon f(e_8)\#\{\gamma_i\}, & \text{if } \gamma_i \text{ is vertical} \end{cases} \tag{3.21}$$

$$E_\varepsilon^{(1)}(\partial_\varepsilon K_u, \delta_j^\alpha \cup \delta_j^\beta) = \varepsilon f(e^3)\#\{\delta_j^\alpha\} + \varepsilon f(e^3)\#\{\delta_j^\beta\} \tag{3.22}$$

Setting $\mathcal{I}_h := \{i : \gamma_i \text{ is horizonthal}\}$ and $\mathcal{I}_v := \{i : \gamma_i \text{ is vertical}\}$, the above leads to

$$\begin{aligned}
& E_\varepsilon^{(1)}(\partial_\varepsilon K_u, [A,B]) \\
\geq\ & \sum_{i\in\mathcal{I}_h} E_\varepsilon^{(1)}(\partial_\varepsilon K_u, \gamma_i) + \sum_{i\in\mathcal{I}_v} E_\varepsilon^{(1)}(\partial_\varepsilon K_u, \gamma_i) + \sum_j E_\varepsilon^{(1)}(\partial_\varepsilon K_u, \delta_j^\alpha \cup \delta_j^\beta) \\
\geq\ & \varepsilon \sum_{i\in\mathcal{I}_h} f(e_3)\#\{\gamma_i\} + \varepsilon \sum_{i\in\mathcal{I}_v} 2f(e^3)\#\{\gamma_i\} + \varepsilon \sum_j \left[f(e^3)\#\{\delta_j^\alpha\} + f(e^3)\#\{\delta_j^\beta\} \right] \qquad (3.23) \\
\geq\ & \varepsilon \sum_{i\in\mathcal{I}_h} f(e^3)\#\{\gamma_i\} + \varepsilon \sum_{i\in\mathcal{I}_v} f(e^3)\#\{\gamma_i\} + \varepsilon \sum_j f(e^3)\#\{\delta_j^\beta\} \\
& + \varepsilon \sum_{i\in\mathcal{I}_h} (f(e_3) - f(e^3))\#\{\gamma_i\} + \varepsilon \sum_{i\in\mathcal{I}_v} f(e^3)\#\{\gamma_i\} + \varepsilon \sum_j f(e^3)\#\{\delta_j^\alpha\} \qquad (3.24) \\
=\ & \varepsilon f(e^3) \left[\sum_{i\in\mathcal{I}_h} \#\{\gamma_i\} + \sum_{i\in\mathcal{I}_v} \#\{\gamma_i\} + \sum_j \#\{\delta_j^\beta\} \right] \\
& + \varepsilon (f(e_3) - f(e^3)) \left[\sum_{i\in\mathcal{I}_h} \#\{\gamma_i\} \right] + \varepsilon f(e^3) \left[\sum_{i\in\mathcal{I}_v} \#\{\gamma_i\} + \sum_j \#\{\delta_j^\alpha\} \right] \\
\geq\ & f(e^3)(x_B - x_A) + (f(e_3) - f(e^3))(x_B - x_{H_1}) + f(e^3)(y_{H_1} - y_A) \qquad (3.25) \\
=\ & f(e_3)(x_B - x_{H_1}) + 2f(e^3)(y_{H_1} - y_A). \qquad (3.26)
\end{aligned}$$

We pause to explain the above computation. The idea is to split the energy of γ_i into two portions: (i) $E_\varepsilon^{(1)}(\gamma_i) \geq f(e^3) + f(e^3)$ for vertical γ_i; and (ii) $E_\varepsilon^{(1)}(\gamma_i) = f(e^3) + (f(e_3) - f(e^3))$ for horizontal γ_i. We then distribute the first portion to $\partial_\varepsilon^1 L_u$ and the second portion to $\partial_\varepsilon^1 K_u$ (from (3.23) to (3.24)). Using (3.18), they are recombined at the end (from (3.25) to (3.26)).

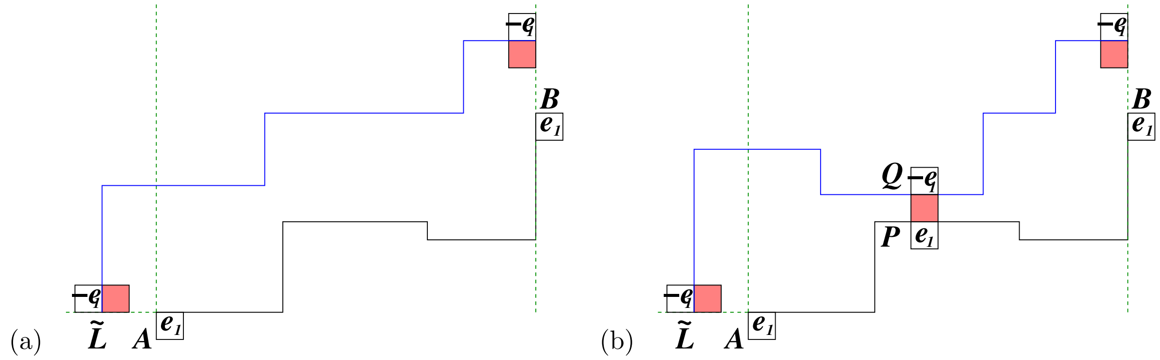

Figure 17: Proof of the appearance of an additional e^3: (a) $\alpha \cap \beta = \emptyset$; (b) $\alpha \cap \beta \neq \emptyset$.

There are two remaining issues.

First, to get the additional $f(e^3)$ as in (3.16), we argue as follows. Consider **Case I**, $\alpha \cap \beta = \emptyset$. Then by slicing along the vertical direction for $[A,B]$, there must be at least an additional energy of $f(e^3)$ to the left of A. For **Case II**, $\alpha \cap \beta \neq \emptyset$, if there is a horizontal γ_i, we proceed from A along $\partial K_u\big|_{[A,B]}$ to the first point P where such a γ_i appears. The same conclusion follows again by slicing in the vertical direction for $[A,P]$. (See Fig. 17.) Note that in both cases, it suffices to consider slicing in the vertical direction as the vector AB or AP are below the bisectrix from A. As the energy of any vertical square from γ_i is $\varepsilon f(e_8)$ which is more than $\varepsilon 2f(e^3)$, the presence of any vertical γ_i can be handled similarly.

By combining the above with (3.12)–(3.15), if H_3 and H_6 are of Type I, then the lower bound can be achieved uniquely by $W_6(K_u)$.

Second, we need to consider the more involved case that H_3 or H_6 are of Type II. Recall that the minimum energy across the e_1 and $-e_1$ interface in the bisectrix direction is achieved by $2f(e^3)$. Note that

$$2f(e^3)N + f(e^3) > 2f(e^3)(N-1) + f(e_8) \quad (\text{since } 3f(e^3) = 6c_2 > 4c_2 + 2c_1 = f(e_8)). \tag{3.27}$$

Hence, if there is just *one more defect* than the necessary $2 \times N$ defects, then the energy is already *higher* than that of $W_6(K_u)$ with a Type II vertex.

To proceed, *suppose that there is no* $\pm e_8$ in $\partial_\varepsilon K_u$. We will show that there must be at least one more defect of e^3 appearing and hence having an e_8 is more advantageous. This is a consequence of the following statements which demonstrate certain "rigidity" of the patterns appearing in a minimizer. Without loss of generality, we consider H_6 being Type II.

1. (This is a more quantitative statement for Fig. 17.) Let $\widetilde{L} \in \varepsilon\mathbb{Z}^2$ be the first lattice point on $y = y_A$ to the left of A such that $w(Q_\varepsilon(\widetilde{L})) = -e_1$. Then by vertical slicing, we have

$$E_\varepsilon^{(1)}\left(\partial_\varepsilon K_u, [A,B]\right) \geq f(e_3)(x_B - x_{H_1}) + 2f(e^3)(y_{H_1} - y_A) + (x_A - x_{\widetilde{L}} - \varepsilon)f(e^3). \tag{3.28}$$

   Hence, if $x_A - x_{\widetilde{L}} \geq 3\varepsilon$, we are done.

2. We must have $u(x_A - \varepsilon, y_A) = u(A)$. Otherwise, $x_A - x_{\widetilde{L}} \geq 3\varepsilon$ and by (1) we are done.

   Similarly, we must also have $u(x_H - \varepsilon, y_H) = u(H)$.

3. By using the connectedness property of ∂K_u, we now analyze the values of u along $\partial K_u|_{[A,H]}$. Let $\{l_s\}_{s\geq 1}$ be the collection of directed segments of $\partial K_u|_{[A,H]}$, each of length ε, starting from A and moving toward H. Without loss of generality, all the vertical segments are pointing downward. We have the following scenarios.

   (a) Let $l_s = [R,S]$ be a vertical segment. Then $u(R) = u(S)$.
   If $u(x_R - \varepsilon, y_R) = -u(R)$, then l_{s+1} must be vertical. Otherwise, $w(x_R - \varepsilon, y_R - \varepsilon) = e_1$, contradicting the fact that $l_s \subset \partial K_u$. We further have $u(x_R - \varepsilon, y_R - \varepsilon) = u(R)$. If $u(x_R - \varepsilon, y_R) = u(R)$, then $u(x_R - \varepsilon, y_R - \varepsilon) = -u(R)$. Otherwise, an $\pm e_8$ will appear, contradicting the assumption of no $\pm e_8$.

   (b) Let $l_s = [R,S]$ is a horizontal segment, pointing to the left ($x_S = x_R - \varepsilon$). Then $u(R) = -u(S)$. Note that there cannot be two consecutive horizontal segments. Otherwise by slicing in the horizontal direction, there will be one more defect and then we are done. Hence, l_{s-1} and l_{s+1} must be both vertical.
   Now let $l_{s-1} = [\widetilde{R}, R]$, and $l_{s+1} = [S, \widetilde{S}]$. Then $u(\widetilde{R}) = u(R)$, $u(S) = u(\widetilde{S})$, $u(x_{\widetilde{R}} - \varepsilon, y_{\widetilde{R}}) = u(\widetilde{R})$. From this, we can deduce that $u(x_S - \varepsilon, y_S) = u(S)$, for otherwise, an additional defect will appear. This also leads to $u(x_{\widetilde{S}} - \varepsilon, y_{\widetilde{S}}) = -u(S)$.
   Similar conclusion holds for horizontal segments pointing to the right.

   (c) (This follows in fact from the previous two statements but is repeated here for emphasis.) The following patterns of a connected sequence of segments *cannot* occur:

   vertical–horizontal(pointing left)–vertical–horizontal(pointing right)-vertical
   or vertical–horizontal(pointing right)–vertical–horizontal(pointing left)-vertical.

   Otherwise, a $\pm e_8$ will appear, contradicting the assumption of no e_8.

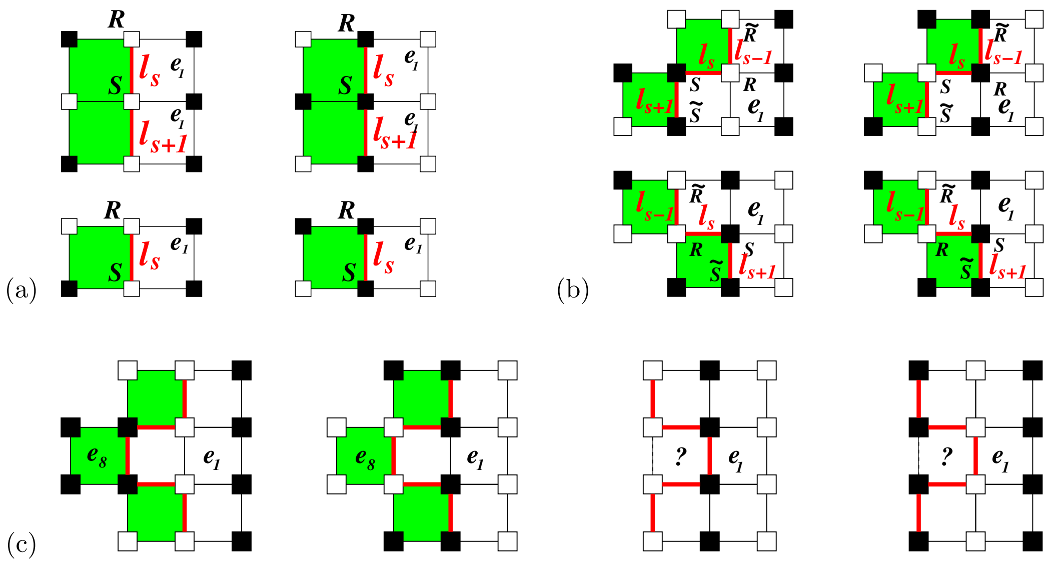

Figure 18: Cases of propagation of spin values along ∂K_u. (a): l_s is a vertical segment; (b): l_s is a horizontal segment; (c): the impossibility of the sequence vertical–horizontal(pointing left)–vertical–horizontal(pointing right)-vertical and vertical–horizontal(pointing right)–vertical–horizontal(pointing left)-vertical. The last two scenarios of (c) contradict the fact that the middle vertical segment is from ∂K_u.

See Fig. 18 for an illustration of the above statements. With the above, we can relate the spin values along the boundary curve ∂K_u. In order to satisfy the above rigidity conditions, starting from A, $\{l_s\}$ can be partitioned into a disjoint sequence of: (i) even number of vertical segments; (ii) vertical–horizontal(left) segments; and (iii) horizontal(right)–vertical segments. This dictates that A and H must be of the same parity, contradicting the initial assumption that the bisectrices at A and H intersect at the center of a square. Hence, an e_8 must appear. $\square$

4 Dynamics of e_1 Inside e_2: $w^\infty = e_2$

The argument in this case follows [10] quite closely. Hence, we will only outline the key steps of the proof. A detailed proof will in fact be given in Section 5 for the more difficult case of interfaces between e_1- and $-e_1$-phases.

First Step. Given an initial spin function u_0 such that K_{u_0} is a Wulff-like rectangle, the minimizer of the functional (2.24) $\mathcal{F}(u_0, \cdot)$ is also a Wulff-like rectangle. The main reason, due to the assumption (H2), $c_2 > c_1$, is that for each e_1 connected component, the interfacial energy must be at least the boundary length (times $f(e^3)$) (this fact in essence is also the main argument used in the proof of Proposition 3.1). Then, upon moving the individual components toward the center and concatenating them together, both the interfacial $E_\varepsilon^{(1)}$ and incremental energies $B_{\varepsilon,\tau}$ in (2.24) must decrease. Hence, we are lead to only one component of e_1-crystal which is a Wulff-like rectangle.

Second Step. With the above characterization of the minimizer, the motion is then completely captured by the distance each bisectrix side moves (see Fig. 19). The actual value for these distances solve a finite-dimensional minimization problem which will be described in more detail in the following.

Given $K_0 = K_{u_0}$, let L_1, L_2, L_3, L_4 be the lengths of the sides of K_0 . Now let N_1, N_2, N_3, N_4 be the

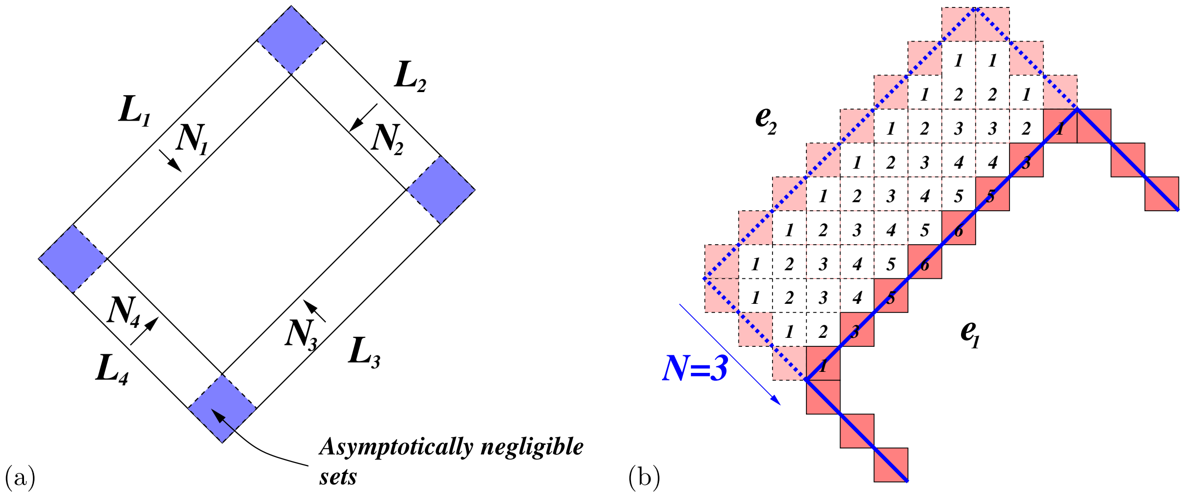

Figure 19: Motion of sets between e_1 and e_2. (a) Continuum description. (b) Discrete representation of (a). The numbers in the squares indicate their L^1-distance to $\partial_\varepsilon K_0$.

number of layers the segments move inward measured along the normal (bisectrix) direction (see Fig. 19). Then we need to minimize:

$$
\begin{aligned}
f(N_1,N_2,N_3,N_4) &= \mathcal{F}_{\varepsilon,\tau}(u_0,v) - E_\varepsilon^{(1)}(K_0) \\
&= -2\left[\varepsilon\sum_{i=1}^{4} f(e^3)N_i\right] + \frac{\varepsilon^2}{\tau}\sum_{\{i\in\varepsilon\mathbb{Z}^2 : w(v)_i\neq w(u_0)_i\}} \mathrm{Dist}_\varepsilon^1\left(Q_\varepsilon(i),\partial_\varepsilon K_{u_0}\right) \\
&= -2\varepsilon\sum_{i=1}^{4} f(e^3)N_i + \frac{\varepsilon}{\alpha}\sum_{i=1}^{4}\left(\sum_{k=1}^{2N_i}\varepsilon k\right)\frac{L_i}{\sqrt{2}\varepsilon} - \frac{\varepsilon^2}{\alpha}e_\varepsilon \\
&= \varepsilon\sum_{i=1}^{4}\left[-2f(e^3)N_i + \frac{N_i(2N_i+1)}{\alpha}\frac{L_i}{\sqrt{2}}\right] - \varepsilon^2 e_\varepsilon. \qquad (4.1)
\end{aligned}
$$

where we have used the facts that: (i) $\tau=\alpha\varepsilon$; (ii) the L^1-distance between two parallel bisectric sides shifted along their normal direction by N cubes (or layers) is given by $2N$ (see Figures 19(b)); (iii) the number of squares along a bisectrix segment with length L is given by $\frac{L}{\sqrt{2}\varepsilon}$. Furthermore, the regions around the vertices lead to an error term $\varepsilon^2 e_\varepsilon$, where it holds

$$
0 < e_\varepsilon \le C\max(N_1,N_2,N_3,N_4)^3.
$$

Hence the error becomes negligible in the limit $\varepsilon\to 0$. The minimizer is characterized by the inequalities

$$
f(\cdots,N_i,\cdots) \le f(\cdots,N_i\pm 1,\cdots), \quad \text{for } i=1,2,3,4.
$$

By the evenness of quadratic function with respect to the minimum point, the optimal value N_i^* of N_i is the integer closest to the following value

$$
\frac{2f(e^3)\alpha\sqrt{2}}{4L_i} - \frac{1}{4} = \left(\frac{f(e^3)\alpha}{\sqrt{2}L_i} + \frac{1}{4}\right) - \frac{1}{2}. \qquad (4.2)
$$

Note the fact that the closest integer to $x-\frac{1}{2}$ is given by $\lfloor x\rfloor$. Hence, upon setting

$$
\widetilde{\kappa}_i = \frac{f(e^3)\alpha}{\sqrt{2}L_i} + \frac{1}{4}, \qquad (4.3)
$$

we then have

$$N_i^* = \lfloor \widetilde{\kappa}_i \rfloor, \qquad \text{if } \operatorname{Dist}(\widetilde{\kappa}_i, \mathbb{N}) \geq \bar{C}\varepsilon; \tag{4.4}$$

$$N_i^* \in \{\lfloor \widetilde{\kappa}_i \rfloor - 1, \lfloor \widetilde{\kappa}_i \rfloor\}, \quad \text{if } \widetilde{\kappa}_i - \lfloor \widetilde{\kappa}_i \rfloor < \bar{C}\varepsilon; \tag{4.5}$$

$$N_i^* \in \{\lfloor \widetilde{\kappa}_i \rfloor, \lfloor \widetilde{\kappa}_i \rfloor + 1\}, \quad \text{if } \lfloor \widetilde{\kappa}_i \rfloor + 1 - \widetilde{\kappa}_i < \bar{C}\varepsilon, \tag{4.6}$$

where $\bar{C} = C(L_1, \ldots, L_4)$ can be bounded as in [10, p. 480]

$$0 \leq C(L_1, \ldots, L_4) \leq \frac{C\alpha^3}{\min(L_1, \ldots, L_4)^4}.$$

As a result each sides will move with *inward normal* velocity given by:

$$V_i = \frac{\sqrt{2}\varepsilon N_i^*}{\tau} = \frac{\sqrt{2} N_i^*}{\alpha}. \tag{4.7}$$

The continuum limit (2.30) is obtained by letting $\varepsilon \longrightarrow 0$.

Note that the definition of $\widetilde{\kappa}_i$ in (4.3) incorporates the factor α while that of κ_i in (2.30), in the statement of Theorem 2.8, does not. The latter is in fact more physical because it coincides with the definition of crystalline curvature in the continuum limit. The use of $\tilde{\kappa}$ is for notational simplicity and will turn out to be particularly convenient in the proof of Theorem 2.10.

We pause here to elaborate formulas (4.4)–(4.6). In the limit $\varepsilon \longrightarrow 0$, if $\widetilde{\kappa}_i \notin \mathbb{N}$, then the number of layers moved for the i-th edge and hence its velocity is uniquely defined by (4.4). But if $\widetilde{\kappa} \in \mathbb{N}$, then the velocity is not uniquely defined. The actual value will depend on the manner, at the ε-level, how $\widetilde{\kappa}_i$ approaches $\mathbb{N}$ (for example, whether it is from above (4.5) or from below (4.6)). When this happens, by the method of continuity, we can actually prescribe the limit in some arbitrary way by imposing $\alpha = \alpha(\varepsilon)$ appropriately. See [1] for detail. A further remark is that since the property $\widetilde{\kappa}_i \notin \mathbb{N}$ is an open set, once the shape falls into this region, it will remain so for some time interval which does not depend on ε.

5 Dynamics of e_1 Inside $-e_1$: $w^\infty = -e_1$

For this case, even with the assumption, $c_2 > c_1$, the situation can be very delicate due to the potential appearance of the $\pm e_2$ phase and the existence of Type I and II vertices for H_3 and H_6.

For the first difficulty, consider the following example that an e_2-phase appears in such a manner to replace part of the original e_1, so that the e_1-crystal becomes disconnected. Note that the energy between e_1 and $-e_1$ in the vertical direction is $f(e_3) = 4c_2 - 2c_1$ and that between e_2 and $-e_1$ is $f(e^3) = 2c_2$. With the standing assumption $c_2 > c_1$, we have $f(e_3) > f(e^3)$. Hence, the presence of e_2-phase might decrease the interfacial energy (see Figures 20). Some global consideration is needed.

For the second difficulty, it will be demonstrated that both Type I and II vertices can appear during the successive minimization process. We need to perform a more careful analysis of the actual motion. It is an interesting type of analysis leading to some further homogenization of the boundary velocity.

5.1 Characterization of Minimizers of $\mathcal{F}_{\varepsilon,\tau}$

Here we prove that given an initial crystal consisting of a Wulff-like hexagon of e_1 inside $-e_1$, the hexagonal shape is preserved at each minimization step.

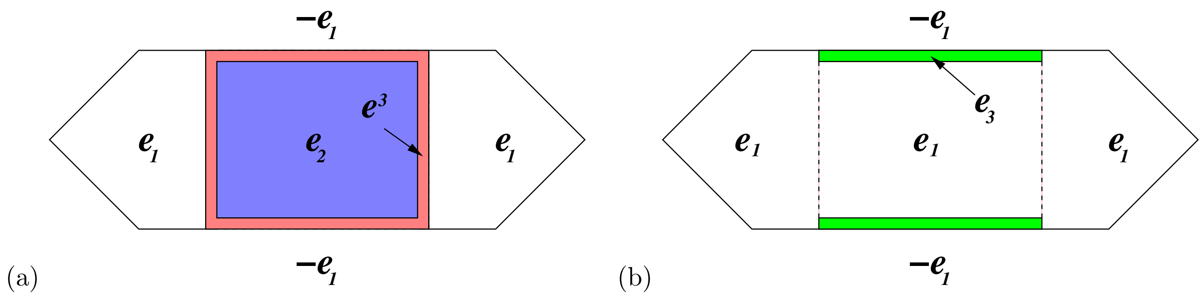

Figure 20: Due to $f(e_3) > f(e^3)$, the introduction of an e_2 phase inside e_1 and $-e_1$ phases (as in (a)) can have an overall smaller interfacial energy than that by direct contact between the e_1 and $-e_1$ phases (as in (b)). Thus some global consideration is needed.

Let the initial condition be given by $u_0 \in \mathcal{S}_\varepsilon^\infty$ such that

$$K_{u_0} = \bigcup \{Q_\varepsilon(i) : w(u_0)_i = e_1\}$$

is a Wulff-like hexagon. As in Definition 2.7, we label the hexagon clockwise, starting from the upper left vertex as $H_1\, H_2\, H_3\, H_4\, H_5\, H_6$. We recall that the energy functional to be minimized at each step is given for $v \in \mathcal{S}_\varepsilon^\infty$ by

$$\mathcal{F}_{\varepsilon,\tau}(v, u_0) \quad = \quad E_\varepsilon^{(1)}(v) + \frac{\varepsilon^2}{\tau} \sum_{\{i \in \varepsilon\mathbb{Z}^2 :\ w(v)_i \neq w(u_0)_i\}} \mathrm{Dist}_\varepsilon^1(Q_\varepsilon(i), \partial_\varepsilon K_{u_0}). \tag{5.1}$$

We will prove that a minimizer is a Wulff-like hexagon, by showing that otherwise there exists a sequence of modifications which turn it into a Wulff-like hexagon possibly decreasing its energy. Essentially, starting from a minimizer w_1, we will produce a finite sequence of pattern functions $\widetilde{w}_m \in \widetilde{W}$ such that $\mathcal{F}_{\varepsilon,\tau}(\widetilde{w}_m) \geq \mathcal{F}_{\varepsilon,\tau}(\widetilde{w}_{m+1})$ and $\widetilde{w}_N = w(v_*)$ for some $v_* \in \mathcal{S}_\varepsilon^\infty$ such that K_{v_*} is a Wulff-like hexagon. It might be the case that the $\widetilde{w}_m$ $(m = 2, 3, \dots N-1)$ is not given by a spin function; i.e., $\widetilde{w}_m \in \widetilde{\mathcal{W}} \backslash \mathcal{W}$, but this will turn out to be irrelevant.

5.1.1 Truncation of the patterns: $\widetilde{w}_2$

First let $w_1 = w(u_1)$ be the pattern function of a minimizer u_1 of (5.1). Suppose K_{u_1} is not a Wulff-like hexagon, we will define a new pattern function $\widetilde{w}_2 \in \widetilde{\mathcal{W}}$ by the following truncation procedure by K_{u_0}:

1. Define $\widetilde{w}_2$ as $\widetilde{w}_2(i) = \begin{cases} w_1(i) & \text{if } Q_\varepsilon(i) \subseteq K_{u_0}, \\ -e_1 & \text{if } Q_\varepsilon(i) \not\subseteq K_{u_0}. \end{cases}$

2. For each square Q_ε just below the line segment $[H_1 H_2]$, let $Q_\varepsilon^{\mathrm{U}}$ be its nearest upper neighhour. Then modify $\widetilde{w}_2(Q_\varepsilon^{\mathrm{U}})$ in the following situations:
   (i) if $\widetilde{w}_2(Q_\varepsilon) = e_1$, then modify $\widetilde{w}(Q_\varepsilon^{\mathrm{U}})$ to be e_3;
   (ii) if $\widetilde{w}_2(Q_\varepsilon) = \pm e_2$, then modify $\widetilde{w}(Q_\varepsilon^{\mathrm{U}})$ to be e^3.

   Perform similar modification of $\widetilde{w}_2$ for squares located just below the segment $[H_4 H_5]$.

3. For each square Q_ε lying on the bisectrix segments $[H_2 H_3]$. Let $Q_{\varepsilon,\mathrm{L}}$ and $Q_{\varepsilon,\mathrm{R}}$ be its left and right neighbours. Then modify $\widetilde{w}_2$ according to the following rules.

Suppose H_3 is a lattice point:
(i) if $\widetilde{w}_2(Q_{\varepsilon,\mathrm{L}}) = e_1$, then modify $\widetilde{w}_2(Q_\varepsilon)$ and $\widetilde{w}_2(Q_{\varepsilon,\mathrm{R}})$ to be e^3;
(ii) if $\widetilde{w}_2(Q_{\varepsilon,\mathrm{L}}) = \pm e_2$, then modify $\widetilde{w}_2(Q_\varepsilon)$ to be e^3.

Suppose H_3 is the center of a square Q^*_ε. Then make the same assignment as above except for Q^*_ε:
(i) if $\widetilde{w}_2(Q^*_{\varepsilon,\mathrm{L}}) = e_1$, then modify $\widetilde{w}_2(Q^*_\varepsilon)$ to be e_8;
(ii) if $\widetilde{w}_2(Q^*_{\varepsilon,\mathrm{L}}) = e_2$, then modify $\widetilde{w}_2(Q^*_\varepsilon)$ to be e_3.

Perform similar modification of $\widetilde{w}_2$ for squares lying on the segments $[H_3H_4]$, $[H_5H_6]$ and $[H_6H_1]$.

4. Consider the four pairs of squares $(Q^{\mathrm{I}}_{\varepsilon,i} \subseteq K_{u_0}, Q^{\mathrm{O}}_{\varepsilon,i} \not\subseteq K_{u_0})$ for $i = 1, 2, 4, 5$ which touch the vertices H_1, H_2, H_4, H_5 and are symmetric across the bisectrix direction. If $\widetilde{w}_2(Q^{\mathrm{I}}_{\varepsilon,i}) = e_1$, then change $\widetilde{w}_2(Q^{\mathrm{O}}_\varepsilon)$ to be e^3.

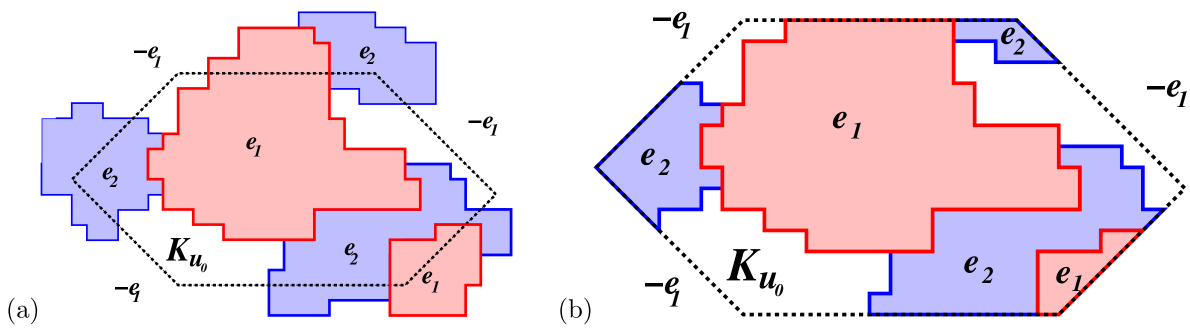

Figure 21: Truncation of w_1 by K_{u_0}, leading to $\widetilde{w}_2$

The procedure above is schematically illustrated in Figure 21. After that, we have

$$\mathcal{F}_{\varepsilon,\tau}(w_1) \geq \mathcal{F}_{\varepsilon,\tau}(\widetilde{w}_2) \tag{5.2}$$

as both the incremental bulk term $B_{\varepsilon,\tau}$ and the interfacial energy term $E^{(1)}_\varepsilon$ are reduced due to the truncation and replacement of the pattern by the minimizing pattern.

5.1.2 Enlargement of e_1-crystal to be Wulff-like hexagon

With the $\widetilde{w}_2$ constructed above, consider its e_1-crystal and its partition into its connected components:

$$\widetilde{K}_2 = \bigcup \{Q_\varepsilon(i) : \widetilde{w}_2(i) = e_1\} = \bigcup_\alpha \widetilde{K}^\alpha_2. \tag{5.3}$$

We will enlarge each $\widetilde{K}^\alpha_2$ to its Wulff-like envelope, $W_6(\widetilde{K}^\alpha_2)$. Then we can estimate the interfacial energy fairly easily. Similar to the definition of L_u in the proof of Proposition 3.2, we define the exterior $\widetilde{L}_2$ to $\widetilde{K}_2$ to be the (unique) unbounded connected component of the set which is the union of the squares with pattern $-e_1$. We further consider the connected components of its boundaries:

$$\partial\widetilde{L}_2 = \bigcup_\beta \partial\widetilde{L}^\beta_2, \quad \partial^1_\varepsilon\widetilde{L}_2 \;=\; \bigcup_\beta \partial^1_\varepsilon\widetilde{L}^\beta_2. \tag{5.4}$$

Note that each of the $\widetilde{K}^\alpha_2$ must be enclosed by one of the $\partial\widetilde{L}^\beta_2$'s. Without loss of generality, we can assume that each $\partial\widetilde{L}^\beta_2$ encloses some $\widetilde{K}^\alpha_2$.

Next, consider first the case that $\partial\widetilde{L}_2$ consists of only one component. For simplicity, we will also omit the subscript 2.

Consider the sets $W_6(\widetilde{L})$, $\partial^1_\varepsilon\widetilde{L}$, $\partial^1_\varepsilon\widetilde{K}$, and $W_6(\widetilde{K}^\alpha)$ for each α. We have the following two cases.

Case I: $\partial^1_\varepsilon\widetilde{L}\bigcap\partial^1_\varepsilon\widetilde{K}=\emptyset$. Then

$$E^{(1)}_\varepsilon(\widetilde{w}_2,\partial^1_\varepsilon\widetilde{L}) \ \geq\ \varepsilon f(e^3)\#\left\{\partial^1_\varepsilon W_6(\widetilde{L})\right\} \tag{5.5}$$

$$E^{(1)}_\varepsilon(\widetilde{w}_2,\partial^1_\varepsilon\widetilde{K}^\alpha) \ \geq\ \varepsilon f(e^3)\#\left\{\partial^1_\varepsilon W_6(\widetilde{K}^\alpha)\right\},\quad \text{for each } \alpha. \tag{5.6}$$

Hence

$$E^{(1)}_\varepsilon\left(\widetilde{w}_2,\partial^1_\varepsilon\widetilde{L}\cup\bigcup_\alpha\partial^1_\varepsilon\widetilde{K}^\alpha\right)\geq\varepsilon f(e^3)\left[\#\left\{\partial^1_\varepsilon W_6(\widetilde{L})\right\}+\sum_\alpha\#\left\{\partial^1_\varepsilon W_6(\widetilde{K}^\alpha)\right\}\right]. \tag{5.7}$$

Case II: $\partial^1_\varepsilon\widetilde{L}\bigcap\partial^1_\varepsilon\widetilde{K}\neq\emptyset$**.** Recalling Figure 16, for each $Q_\varepsilon\in\partial^1_\varepsilon\widetilde{L}\bigcap\partial^1_\varepsilon\widetilde{K}$, we have the following two cases:

1. $\widetilde{w}_2(Q_\varepsilon)=e_8$ in which case it connects a $-e_1$ to an e_1 horizontally through one square. As $f(e_8)=4c_2+2c_1>4c_2=2f(e^3)$, we will decompose the value of $f(e_8)$ into two $f(e^3)$'s and associate one $f(e^3)$ to $\partial^1_\varepsilon\widetilde{L}$ and one $f(e^3)$ to $\partial^1_\varepsilon\widetilde{K}$.

2. $\widetilde{w}_2(Q_\varepsilon)=e_3$ in which case it connects a $-e_1$ to an e_1 vertically through one square. As $f(e_3)=4c_2-2c_1$, we will decompose the value of $f(e_3)$ into $f(e^3)=2c_2$ that we associate to $\partial^1_\varepsilon\widetilde{L}$ and $f(e_3)-f(e^3)=2c_2-2c_1(>0)$ that we associate to $\partial^1_\varepsilon\widetilde{K}$.

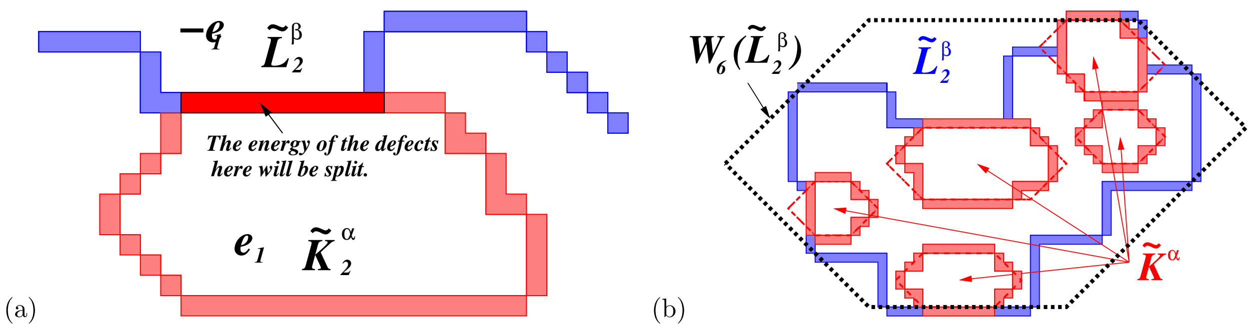

Figure 22: (a) Splitting of energy: $f(e_3)=f(e^3)+(2c_2-2c_1)$; (b) Enlargement of e_1-crystals.

Then we have the following lower bound,

$$E^{(1)}_\varepsilon\left(\widetilde{w}_2,\partial^1_\varepsilon\widetilde{L}\cup\bigcup_\alpha\partial^1_\varepsilon\widetilde{K}^\alpha\right)\geq\varepsilon f(e^3)\#\left\{\partial^1_\varepsilon W_6(\widetilde{L})\right\}+\sum_\alpha E^{(1),-}_\varepsilon\left(\partial^1_\varepsilon W_6(\widetilde{K}^\alpha)\right) \tag{5.8}$$

where $E^{(1),-}_\varepsilon$ is the interfacial energy which gives a weight $f(e^3)$ to sides with bisectrix normals and $f(e_3)-f(e^3)$ to sides with vertical normals. (The above idea of splitting the energy has already appeared once in the derivation of (3.26). See also the explanation right below (3.26).) See Fig. 22(a,b) for an illustration of this step. Combining (5.7) and (5.8), and extending to the case with multiple components of $\partial\widetilde{L}^\beta$'s, we conclude that

$$E^{(1)}_\varepsilon(\widetilde{w}_2) \ \geq\ E^{(1)}_\varepsilon\left(\widetilde{w}_2,\partial^1_\varepsilon\widetilde{L}\cup\bigcup\partial^1_\varepsilon\widetilde{K}\right) \tag{5.9}$$

$$\geq\ \varepsilon f(e^3)\sum_\beta\#\left\{\partial^1_\varepsilon W_6(\widetilde{L}^\beta)\right\}+\sum_\alpha E^{(1),-}_\varepsilon\left(\partial^1_\varepsilon W_6(\widetilde{K}^\alpha)\right). \tag{5.10}$$

In summary, the interfacial energy of $\widetilde{w}_2$ is bounded below by the sum of two contributions:

(i) the first comes from the boundary of Wulff-like hexagons $W_6(\partial_\varepsilon^1 \widetilde{L}^\beta))$ – their energy is the number of squares weighted by $\varepsilon f(e^3)$; and

(ii) the second comes from the boundary of Wulff-like hexagons $\partial_\varepsilon^1 \widetilde{K}^\alpha$ – their energy is the number of squares weighted by $\varepsilon f(e^3)$ for the bisectrix normal direction and $\varepsilon(f(e_3) - f(e^3))$ (> 0) for the vertical normal direction.

5.1.3 Movement and concatenation of components of e_1: $\widetilde{w}_3$

Now consider the incremental bulk term:

$$\begin{aligned}
B_{\varepsilon,\tau}(\widetilde{K}_2) &= \int_{\{\bigcup Q_\varepsilon(i):\ \widetilde{w}_{2,i} \neq w(u)_i\}} \mathrm{Dist}_\varepsilon^1(x, \partial K_{u_0})\, dx = \int_{K_{u_0} \setminus \widetilde{K}_2} \mathrm{Dist}_\varepsilon^1(x, \partial K_{u_0})\, dx \\
&= \int_{K_{u_0}} \mathrm{Dist}_\varepsilon^1(x, \partial K_{u_0})\, dx - \int_{\widetilde{K}_2} \mathrm{Dist}_\varepsilon^1(x, \partial K_{u_0})\, dx \\
&= \int_{K_{u_0}} \mathrm{Dist}_\varepsilon^1(x, \partial K_{u_0})\, dx - \int_{\bigcup_\alpha \widetilde{K}_2^\alpha} \mathrm{Dist}_\varepsilon^1(x, \partial K_{u_0})\, dx \\
&\geq \int_{K_{u_0}} \mathrm{Dist}_\varepsilon^1(x, \partial K_{u_0})\, dx - \int_{\bigcup_\alpha W_6(\widetilde{K}_2^\alpha)} \mathrm{Dist}_\varepsilon^1(x, \partial K_{u_0})\, dx
\end{aligned}$$

(where we have used the formulation (2.25)). Note that the first integral of the two last integrals is a fixed quantity independent of $\widetilde{K}_2$ while the second is more negative if the component is nearer to the center of K_{u_0}. *Hence, it is more advantageous to move each e_1-component of $\widetilde{K}_2$ toward the center.*

We now modify $\widetilde{w}_2$ according to the reasoning above.

1. Inside each $\partial_\varepsilon^1 W_6(\widetilde{L}^\beta)$, we can move each component $\widetilde{K}^\alpha$ toward the center. When they touch, we can replace the new connected component by its Wulff-like envelope. This step can reduce both the interfacial energy $E_\varepsilon^{(1)}$ and the incremental bulk term B as:

$$\begin{aligned}
\bigcup_\alpha W_6(\widetilde{K}^\alpha) \quad &\subseteq \quad W_6\Big(\bigcup_\alpha \widetilde{K}^\alpha\Big), \\
\text{and} \quad E_\varepsilon^{(1),-}\left(\bigcup_\alpha \partial_\varepsilon^1 W_6(\widetilde{K}^\alpha)\right) \quad &\geq \quad E_\varepsilon^{(1),-}\left(\partial_\varepsilon^1 W_6\left(\bigcup_\alpha \widetilde{K}^\alpha\right)\right).
\end{aligned}$$

   The above combined movement, concatenation and enlargement procedures lead to one single e_1-crystal $\widetilde{W_6}(\beta)$ which is a Wulff-like hexagon. At the same time, we will shrink the size of $\widetilde{W_6}\left(\partial_\varepsilon^1 \widetilde{L}^\beta\right)$ until it is equal to $\widetilde{W_6}(\beta)$.

2. Now we define $\widetilde{w}_3$:

$$\widetilde{w}_3(Q_\varepsilon) = \begin{cases} e_1, & \text{if } Q_\varepsilon \subseteq \widetilde{W_6}(\beta), \\ -e_1, & \text{if } Q_\varepsilon \not\subseteq \widetilde{W_6}(\beta) \end{cases}. \tag{5.11}$$

   Then we modify $\widetilde{w}_3$ on the boundary of $W_6(\beta)$ to be the minimum pattern dictated by Lemma 2.4 and taking into consideration of the necessary modification for Type II vertices. As $f(e_3) = 4c_2 - 2c_1 = f(e^3) + 2c_2 - 2c_1$, the splitting of the energy of e_3 can be recombined. Hence, we have

$$E_\varepsilon^{(1)}(\widetilde{w}_2) \geq E_\varepsilon^{(1)}\left(\widetilde{w}_3, \partial_\varepsilon \widetilde{W_6}(\beta)\right) \tag{5.12}$$

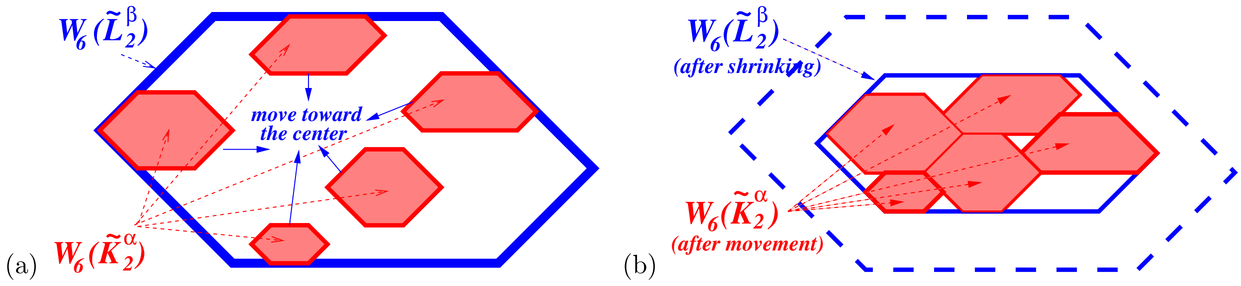

Figure 23: (a) Movement toward the center and (b) concatenation of the e_1-crystal components in $\widetilde{w}_2$, leading to $\widetilde{w}_3$

3. Perform the same procedure for each $\partial_\varepsilon^1 W_6(\widetilde{L}^\beta)$. Ultimately, we are led to only one component of the e_1-crystal which is a Wulff-like hexagon (see Fig. 23(a,b)).

The above procedures lead to the conclusion: *Given an initial K_{u_0} which is a Wulff-like hexagon, then the minimizer v^* of the functional $\mathcal{F}_{\varepsilon,\tau}(\cdot, u_0)$ is also given by a Wulff-like hexagon contained in K_{u_0}.*

5.2 Motion of Wulff Like Hexagonal - with Type I and II Hexagons

Here we give the motion law for the interface between e_1 and $-e_1$. As to be seen, the continuum description of the motion of the (bisectrix) segments depends on the transition between the Type I and Type II vertices in Wulff-like hexagon.

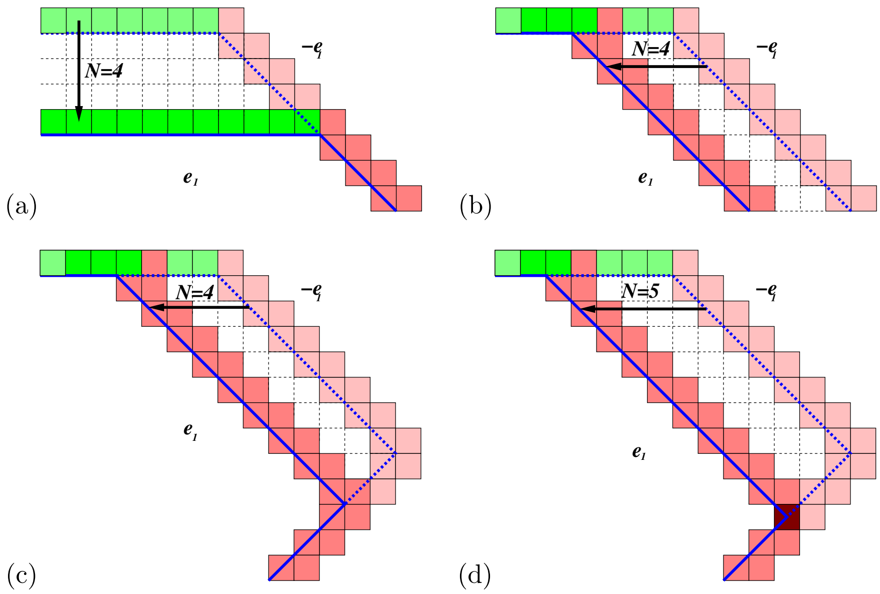

Figure 24: Motion of sides for Wulff-like Hexagons

Let $K_0 = K_{u_0}$ be a Wulff-like hexagon (which can contain both Types I and II vertices). We use the same notation as in Definition 2.7. Let $L_1, L_2, \ldots L_6$ be the lengths of the sides of the hexagon, with $L_i = |H_i H_{i+1}|$ ($H_7 = H_1$). Let further N_1, N_4 be the number of layers the horizontal segments L_1 and L_4 move inward measured along the normal (vertical) direction, and N_2, N_3, N_5, N_6 be the number of layers the bisectrix segments L_2, L_3, L_5, and L_6 move inwards measured along the horizontal directions (see Fig. 24)[2]. The actual functional to be minimized depends on whether the vertices H_3 and H_6 are of Type I or Type II. It can be derived as:

$$
\begin{aligned}
f(N_1, N_2, \ldots, N_6) &= \frac{1}{\varepsilon}\left[\mathcal{F}_{\varepsilon,\tau}(v, u_0) - E_\varepsilon^{(1)}(u_0)\right] \\
&= \frac{1}{\varepsilon}\left[E_\varepsilon^{(1)}(v) - E_\varepsilon^{(1)}(u_0) + \frac{\varepsilon^2}{\tau}\sum_{\{i\in\mathbb{Z}^2 : w(v)_i \neq w(u_0)_i\}} \mathrm{Dist}_\varepsilon^1\left(Q_\varepsilon(i), \partial_\varepsilon K_0\right)\right] \\
&= \frac{1}{\varepsilon}\left[E_\varepsilon^{(1)}(v) - E_\varepsilon^{(1)}(u_0) + \frac{\varepsilon^2}{\tau}\sum_{i=1,4}\left(\sum_{k=1}^{N_i}\varepsilon k\right)\frac{L_i}{\epsilon} + \frac{\varepsilon^2}{\tau}\sum_{i=2,3,5,6}\left(\sum_{k=1}^{N_i}\varepsilon k\right)\frac{L_i}{\epsilon\sqrt{2}} + \varepsilon^2 e_\varepsilon\right] \\
&= \frac{1}{\varepsilon}\left[E_\varepsilon^{(1)}(v) - E_\varepsilon^{(1)}(u_0)\right] + \frac{1}{\alpha}\sum_{i=1,4}\frac{N_i(N_i+1)}{2}L_i + \frac{1}{\alpha}\sum_{i=2,3,5,6}\frac{N_i(N_i+1)}{2}\frac{L_i}{\sqrt{2}} + \varepsilon e_\varepsilon \\
&= \sum_{i=1}^{6} g_i(N_i) + s(H_3)2c_1\mathrm{Par}(N_2+N_3) + s(H_6)2c_1\mathrm{Par}(N_5+N_6) + \varepsilon e_\varepsilon, \qquad (5.13)
\end{aligned}
$$

where

$$
\begin{aligned}
g_i(N_i) &= -2\beta_1 N_i + \frac{m_1}{\alpha}N_i(N_i+1)L_i, \ \ \beta_1 = 2f(e^3), \ \ m_1 = \frac{1}{2}, \ \ i = 1, 4; \\
g_i(N_i) &= -\beta_2 N_i + \frac{m_2}{\alpha}N_i(N_i+1)L_i, \ \ \beta_2 = f(e_3), \ \ m_2 = \frac{1}{2\sqrt{2}} \ \ i = 2, 3, 5, 6; \\
\mathrm{Par}(M) &= 1 \text{ if } M \text{ is a odd and } 0 \text{ if } M \text{ is even}; \\
s(H) &= 1 \text{ if } H \text{ is Type I and } -1 \text{ if } H \text{ is Type II}; \\
|e_\varepsilon| &\leq C\left(N_1 + \cdots + N_6\right)^3.
\end{aligned}
$$

The appearance of $\mathrm{Par}(\cdot)$ and $s(H)$ is explained as follows. Consider the vertex H_3. (The explanation is the same for H_6.) Suppose initially H_3 is Type I; i.e., it is a lattice point. If $N_2 + N_3$ is even, then the new vertex H_3' will still be a Type I vertex. On the other hand, if $N_2 + N_3$ is odd, then the new vertex H_3' is of Type II. The defect e_8 leads to an extra energy of $f(e_8) - 2f(e^3) = 2c_1$, leading to $s(H_3) = 1$. Similarly, if initially H_3 is Type II; i.e., it is the center of a square. Now if $N_2 + N_3$ is odd, then H_3' becomes a Type I vertex. The defect e_8 disappears and hence a reduction of $f(e_8) - 2f(e^3) = 2c_1$ leading to $s(H_3) = -1$.

Note that in the above functional, N_1 and N_4 are decoupled from N_2, N_3, N_5 and N_6. Hence, upon minimization, similar to the reasoning going from (4.1) to (4.4), we obtain the following optimal values for N_1 and N_4 for f:

$$
N_1^* = \left\lfloor \frac{\alpha\beta_1}{m_1 L_1} \right\rfloor \ \text{ and } \ N_4^* = \left\lfloor \frac{\alpha\beta_1}{m_1 L_4} \right\rfloor. \qquad (5.14)
$$

Next, we find the optimal values of N_2 and N_3. (The consideration is the same for N_5 and N_6.) Note that in the functional f above, N_2 and N_3 are coupled together but decoupled from the rest. Now let N_2^* and N_3^* be the minimum points of g_2 and g_3:

$$
N_2^* = \left\lfloor \frac{\alpha\beta_2}{2m_2 L_2} \right\rfloor, \ \text{ and } \ N_3^* = \left\lfloor \frac{\alpha\beta_2}{2m_2 L_3} \right\rfloor. \qquad (5.15)
$$

[2]Note that there is a difference in the definition of the number of layers moving in for the bisectrix segments between the e_1-e_2-interface in Section 4 and the current e_1-$-e_1$-interface. In the former case, the number is measured along the normal bisectrix direction while here it is measured along the horizontal direction. This is simply for arithmetic convenience.

We will incorporate the presence of $s(H_3)\text{Par}(N_2+N_3)$ by considering the following variation:

$$\begin{aligned} h(p,q) &= g_2(N_2^*+p)+g_3(N_3^*+q)+s(H_3)2c_1\text{Par}(N_2^*+p+N_3^*+q) \\ &\quad -[g_2(N_2^*)+g_3(N_3^*)+s(H_3)2c_1\text{Par}(N_2^*+N_3^*)] \\ &= [g_2(N_2^*+p)+g_3(N_3^*+q)-g_2(N_2^*)-g_3(N_3^*)] \qquad (5.16) \\ &\quad +s(H_3)2c_1\left[\text{Par}(N_2^*+N_3^*+p+q)-\text{Par}(N_2^*+N_3^*)\right] \qquad (5.17) \end{aligned}$$

for $p,q\in\{-1,0,1\}$.

Now we separately consider the following two cases.

5.2.1 Case I: H_3 is a Type I vertex; i.e., $s(H_3)=1$.

First note that since N_2^* and N_3^* are the unique minimum points of g_2 and g_3, the term (5.16) is always non-negative.

If $N_2^*+N_3^*$ is even, then (5.17) is also non-negative. Hence, N_2^* and N_3^* are the true minima of f.

If $N_2^*+N_3^*$ is odd, then we have

$$\begin{aligned} & h(N_2^*+p,N_3^*+q) \\ =\ & [g_2(N_2^*+p)+g_3(N_3^*+q)-g_2(N_2^*)-g_3(N_3^*)]+2c_1\left[\text{Par}(N_2^*+N_3^*+p+q)-1\right] \\ =\ & -\beta_2 p-\beta_2 q+\frac{m_2L_2}{\alpha}\left(2pN_2^*+p(p+1)\right)+\frac{m_2L_3}{\alpha}\left(2qN_3^*+q(q+1)\right)-2c_1\text{Par}(p+q). \qquad (5.18) \end{aligned}$$

It suffices to just compare $(p,q)=(0,0)$ with $(p,q)=(\pm1,0)$ or $(0,\pm1)$ so that $-2c_1\text{Par}(p+q)$ is strictly negative. We then have

$$\begin{aligned} h(0,0) &= 0, && (5.19) \\ h(-1,0) &= \beta_2+\frac{m_2L_2}{\alpha}(-2N_2^*)-2c_1, && (5.20) \\ h(1,0) &= -\beta_2+\frac{m_2L_2}{\alpha}(2N_2^*+2)-2c_1, && (5.21) \\ h(0,-1) &= \beta_2+\frac{m_2L_3}{\alpha}(-2N_3^*)-2c_1, && (5.22) \\ h(0,1) &= -\beta_2+\frac{m_2L_3}{\alpha}(2N_3^*+2)-2c_1. && (5.23) \end{aligned}$$

For the following, we denote:

$$\begin{aligned} &\tilde\kappa_2=\frac{\alpha\beta_2}{2m_2L_2},\ \ \tilde\kappa_2=m+s\ \text{ where } \lfloor\tilde\kappa_2\rfloor=m, \text{ and } 0\le s<1, && (5.24) \\ &\tilde\kappa_3=\frac{\alpha\beta_2}{2m_2L_3},\ \ \tilde\kappa_3=n+t\ \text{ where } \lfloor\tilde\kappa_3\rfloor=n, \text{ and } 0\le t<1, && (5.25) \\ &\mathbf{C}(m,n)=\left\{(\tilde\kappa_2,\tilde\kappa_3): m\le\tilde\kappa_2<m+1, n\le\tilde\kappa_3<n+1\right\}. && (5.26) \end{aligned}$$

Note that the α factor is incorporated in the definition of $\tilde\kappa_2$ and $\tilde\kappa_3$. This is in accord with the convention explained for the definition of $\tilde\kappa_i$ in (4.3).

Comparison between $h(-1,0), h(1,0), h(0,-1)$ and $h(0,-1)$. Note that

$$\begin{aligned} h(-1,0)<h(1,0) &\iff \tilde\kappa_2<\lfloor\tilde\kappa_2\rfloor+\frac{1}{2}, && (5.27) \\ h(0,-1)<h(0,1) &\iff \tilde\kappa_3<\lfloor\tilde\kappa_3\rfloor+\frac{1}{2}. && (5.28) \end{aligned}$$

We then subdivide the square $\mathbf{C}(m,n)$ into the following four regions.

lower left $= \left\{0 < s, t < \frac{1}{2}\right\} = \left\{(\tilde{\kappa}_2, \tilde{\kappa}_3) : \tilde{\kappa}_2 < \lfloor\tilde{\kappa}_2\rfloor + \frac{1}{2},\ \tilde{\kappa}_3 < \lfloor\tilde{\kappa}_3\rfloor + \frac{1}{2}\right\}$:

$$h(-1,0) < h(0,-1) \Longleftrightarrow \frac{\lfloor\tilde{\kappa}_3\rfloor}{\tilde{\kappa}_3} < \frac{\lfloor\tilde{\kappa}_2\rfloor}{\tilde{\kappa}_2} \Longleftrightarrow \frac{n}{m}s < t; \tag{5.29}$$

lower right $= \left\{\frac{1}{2} < s < 1,\ 0 < t < \frac{1}{2}\right\} = \left\{(\tilde{\kappa}_2, \tilde{\kappa}_3) : \tilde{\kappa}_2 > \lfloor\tilde{\kappa}_2\rfloor + \frac{1}{2},\ \tilde{\kappa}_3 < \lfloor\tilde{\kappa}_3\rfloor + \frac{1}{2}\right\}$:

$$h(1,0) < h(0,-1) \Longleftrightarrow \frac{\lfloor\tilde{\kappa}_2\rfloor + 1}{\tilde{\kappa}_2} + \frac{\lfloor\tilde{\kappa}_3\rfloor}{\tilde{\kappa}_3} < 2, \Longleftrightarrow \frac{m+1}{m+s} + \frac{n}{n+t} < 2; \tag{5.30}$$

upper right $= \left\{\frac{1}{2} < s, t < 1\right\} = \left\{(\tilde{\kappa}_2, \tilde{\kappa}_3) : \tilde{\kappa}_2 > \lfloor\tilde{\kappa}_2\rfloor + \frac{1}{2},\ \tilde{\kappa}_3 > \lfloor\tilde{\kappa}_3\rfloor + \frac{1}{2}\right\}$:

$$h(1,0) < h(0,1) \Longleftrightarrow \frac{\lfloor\tilde{\kappa}_2\rfloor + 1}{\tilde{\kappa}_2} < \frac{\lfloor\tilde{\kappa}_3\rfloor + 1}{\tilde{\kappa}_3} \Longleftrightarrow t < \frac{n+1}{m+1}s + \frac{m-n}{m+1}; \tag{5.31}$$

upper left $= \left\{0 < s < \frac{1}{2},\ \frac{1}{2} < t < 1\right\} = \left\{(\tilde{\kappa}_2, \tilde{\kappa}_3) : \tilde{\kappa}_2 < \lfloor\tilde{\kappa}_2\rfloor + \frac{1}{2},\ \tilde{\kappa}_3 > \lfloor\tilde{\kappa}_3\rfloor + \frac{1}{2}\right\}$:

$$h(-1,0) < h(0,1) \Longleftrightarrow 2 < \frac{\lfloor\tilde{\kappa}_2\rfloor}{\tilde{\kappa}_2} + \frac{\lfloor\tilde{\kappa}_3\rfloor + 1}{\tilde{\kappa}_3} \Longleftrightarrow 2 < \frac{m}{m+s} + \frac{n+1}{n+t}. \tag{5.32}$$

Comparison of $h(\pm1,0)$ and $h(0,\pm1)$ with $h(0,0)$. This leads to

$$h(-1,0) < h(0,0) \quad \Longleftrightarrow \quad \left(1 - \frac{2c_1}{\beta_2}\right)\tilde{\kappa}_2 < \lfloor\tilde{\kappa}_2\rfloor, \tag{5.33}$$

$$h(1,0) < h(0,0) \quad \Longleftrightarrow \quad \lfloor\tilde{\kappa}_2\rfloor + 1 < \left(1 + \frac{2c_1}{\beta_2}\right)\tilde{\kappa}_2, \tag{5.34}$$

$$h(0,-1) < h(0,0) \quad \Longleftrightarrow \quad \left(1 - \frac{2c_1}{\beta_2}\right)\tilde{\kappa}_3 < \lfloor\tilde{\kappa}_3\rfloor, \tag{5.35}$$

$$h(0,1) < h(0,0) \quad \Longleftrightarrow \quad \lfloor\tilde{\kappa}_3\rfloor + 1 < \left(1 + \frac{2c_1}{\beta_2}\right)\tilde{\kappa}_3 \tag{5.36}$$

In order for $h(0,0) < \min\{h(\pm1,0), h(0,\pm1)\}$, $(\tilde{\kappa}_2, \tilde{\kappa}_3)$ must satisfy

$$\frac{\lfloor\tilde{\kappa}_2\rfloor}{1-\delta} < \tilde{\kappa}_2 < \frac{\lfloor\tilde{\kappa}_2\rfloor + 1}{1+\delta} \text{ and } \frac{\lfloor\tilde{\kappa}_3\rfloor}{1-\delta} < \tilde{\kappa}_3 < \frac{\lfloor\tilde{\kappa}_3\rfloor + 1}{1+\delta} \quad \left(\text{where } \delta = \frac{2c_1}{\beta_2} \in (0,1)\right) \tag{5.37}$$

For convenience, we define the following set to capture the condition (5.37). For any $m, n \in \mathbb{N}$,

$$\mathbf{V}(m,n) = \left(\frac{\delta m}{1-\delta}, \frac{1-m\delta}{1+\delta}\right) \times \left(\frac{\delta n}{1-\delta}, \frac{1-n\delta}{1+\delta}\right). \tag{5.38}$$

Note that $\mathbf{V}$ is a rectangle with the horizontal and vertical lengths given by $\frac{1-(2m+1)\delta}{1-\delta^2}$ and $\frac{1-(2n+1)\delta}{1-\delta^2}$, both of which decrease as m and n increase. Furthermore,

$$\mathbf{V}(m,n) \neq \emptyset \text{ if and only if } m, n < \frac{1-\delta}{2\delta}, \tag{5.39}$$

in particular, $\mathbf{V}(m,n) = \emptyset$ for m, n are large enough.

If for simplicity, we use (5.29)–(5.32) to also refer to the equations of the boundary of the regions; i.e., the equations when equalities hold in the conditions, then they satisfy the following more "refined" properties. (We assume $m \geq n$ and use s and t as our variables.)

1. Equation (5.29), (5.30), (5.31) and (5.32) pass through the points $(0,0),(1,0),(1,1)$ and $(0,1)$ respectively.

2. Equation (5.29) and (5.30) intersect at $s=\frac{1}{2}$ and $t_1=\frac{n}{2m}$ while equation (5.31) and (5.32) intersect at $s=\frac{1}{2}$ and $t_2=\frac{m-\frac{n}{2}+\frac{1}{2}}{m+1}$. (Note $t_1 \le t_2$ for $m \ge n$ and equality holds if and only if $m=n$.)

3. The curves described by (5.29)–(5.32) continue across $\mathbf{C}(m,n)$ in the following sense:

$$\begin{aligned}
(5.29) \text{ for } \mathbf{C}(m,n) &= (5.31) \text{ for } \mathbf{C}(m-1,n-1), && (5.40)\\
(5.30) \text{ for } \mathbf{C}(m,n) &= (5.32) \text{ for } \mathbf{C}(m+1,n-1), && (5.41)\\
(5.31) \text{ for } \mathbf{C}(m,n) &= (5.29) \text{ for } \mathbf{C}(m+1,n+1), && (5.42)\\
(5.32) \text{ for } \mathbf{C}(m,n) &= (5.30) \text{ for } \mathbf{C}(m-1,n+1). && (5.43)
\end{aligned}$$

4. Suppose $\mathbf{V}(m,n) \neq \emptyset$, then its four vertices:

$$A=\left(\tfrac{\delta m}{1-\delta},\tfrac{\delta n}{1-\delta}\right),\quad B=\left(\tfrac{1-\delta m}{1+\delta},\tfrac{\delta n}{1-\delta}\right),\quad C=\left(\tfrac{1-\delta m}{1+\delta},\tfrac{1-\delta n}{1+\delta}\right),\quad D=\left(\tfrac{\delta m}{1-\delta},\tfrac{1-\delta n}{1+\delta}\right) \tag{5.44}$$

   lie on (5.29), (5.30), (5.31) and (5.32) respectively.

The above properties are illustrated in Figures 25 and 26.

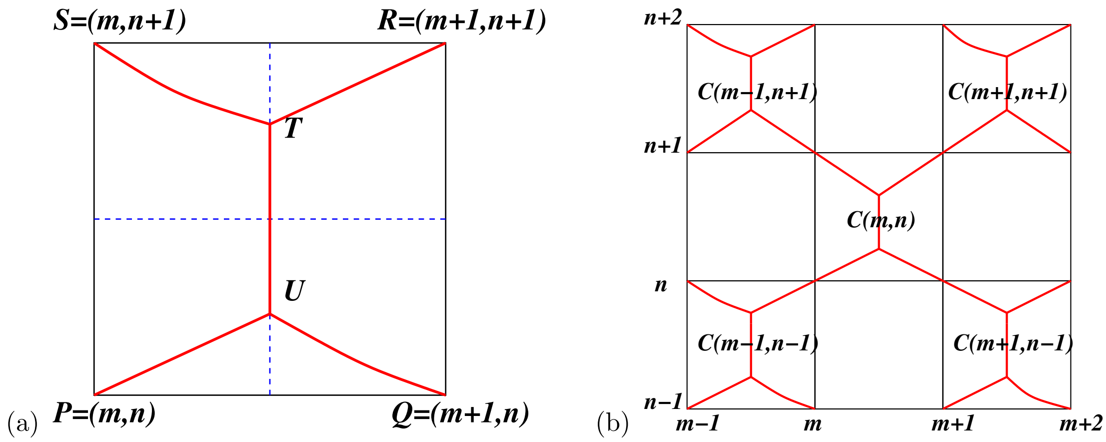

Figure 25: Partitioning of $\mathbf{C}(m,n)$. In (a), the curves (5.29) (PU), (5.30) (QU), (5.31) (RT), (5.32) (ST), and their intersections are shown. The points T and U are equal to $\left(\frac{1}{2},\frac{m-\frac{n}{2}+\frac{1}{2}}{m+1}\right)$ and $\left(\frac{1}{2},\frac{n}{2m}\right)$. In (b), the continuation of the curves (5.29)–(5.32) from $\mathbf{C}(m,n)$ to $\mathbf{C}(m-1,n-1)$, $\mathbf{C}(m+1,n-1)$, $\mathbf{C}(m+1,n+1)$, $\mathbf{C}(m-1,n+1)$ are illustrated.

5.2.2 Case II: H_3 is a Type II vertex; i.e., $s(H_3)=-1$.

This case is basically the same as the previous one except that the cases for $N_2^*+N_3^*$ are even and odd are switched. To be precise, we re-write (5.16)-(5.17) here:

$$\begin{aligned}
h(p,q) &= \left[g_2(N_2^*+p)+g_3(N_3^*+q)-g_2(N_2^*)-g_3(N_3^*)\right]\\
&\quad -2c_1\left[\mathrm{Par}(N_2^*+N_3^*+p+q)-\mathrm{Par}(N_2^*+N_3^*)\right].
\end{aligned}$$

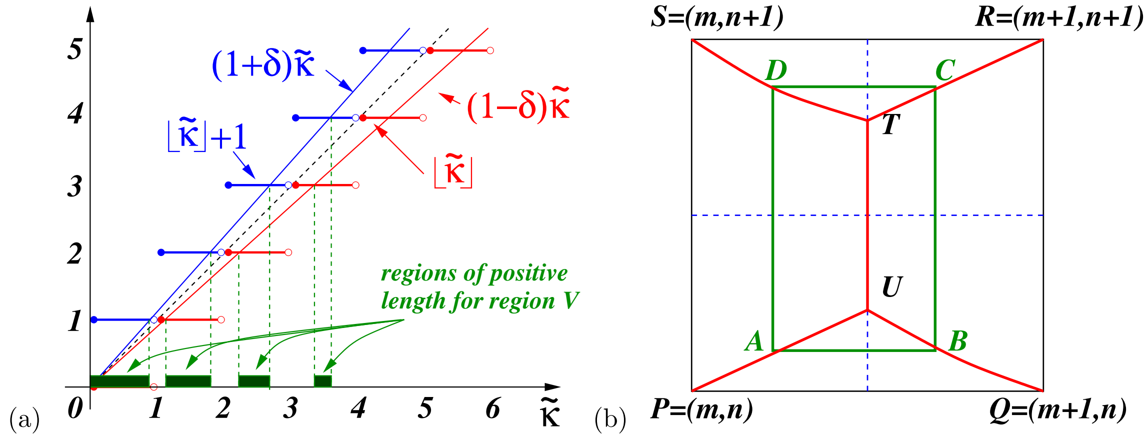

Figure 26: The computation leading to region $\mathbf{V}(m,n)$. In (a), (5.37) is illustrated. The shaded intervals are those values of $\tilde{\kappa}$ such that $h(0,0) < \min\{h(\pm 1,0), h(0,\pm 1)\}$. In (b), the rectangle $\mathbf{V}(m,n)$ (5.38) and its four vertices A, B, C, and D (5.44) are shown.

If $N_2^* + N_3^*$ is odd, then N_2^* and N_3^* give the true minimum of f.

If $N_2^* + N_3^*$ is even, then $h(p,q)$ becomes:

$$h(p,q) \quad = \quad [g_2(N_2^*+p) + g_3(N_3^*+q) - g_2(N_2^*) - g_3(N_3^*)] - 2c_1 \mathrm{Par}(p+q) \tag{5.45}$$

which is the same as (5.18). Then all the definitions of **Regions I–IV** and **V** are the same as before.

5.2.3 Summary for the Minima of (5.17)

First, for any $L_2 = |H_2H_3|$, and $L_3 = |H_3H_4| > 0$, let

$$\tilde{\kappa}_2 = \frac{\alpha\beta_2}{2m_2L_2}, \qquad m = \lfloor \tilde{\kappa}_2 \rfloor, \quad s = \tilde{\kappa}_2 - m;$$
$$\tilde{\kappa}_3 = \frac{\alpha\beta_2}{2m_2L_3}, \qquad n = \lfloor \tilde{\kappa}_3 \rfloor, \quad t = \tilde{\kappa}_3 - n.$$

Now for $m \geq n$, the minima $(N_2^{**}, N_3^{**}) = (N_2^{**}(\tilde{\kappa}_2,\tilde{\kappa}_3), N_3^{**}(\tilde{\kappa}_2,\tilde{\kappa}_3))$ of (5.17) are given by:

$$(m+p, n+q), \tag{5.46}$$

where

(Region V) $(p,q) = (0,0)$: if

$$(s,t) \in \mathbf{V}(m,n) = \left(\frac{\delta m}{1-\delta}, \frac{1-m\delta}{1+\delta}\right) \times \left(\frac{\delta n}{1-\delta}, \frac{1-n\delta}{1+\delta}\right), \quad \left(\delta = \frac{2c_1}{\beta_2}\right); \tag{5.47}$$

(Region I) $(p,q) = (0,-1)$: if

$$(m,n) \notin \mathbf{V}(m,n), \;\; \text{and} \;\; t < \frac{1}{2}, \;\; \frac{n}{m}s > t, \;\; \frac{m+1}{m+s} + \frac{n}{n+t} > 2; \tag{5.48}$$

(Region II) $(p,q) = (1,0)$: if

$$(m,n) \notin \mathbf{V}(m,n), \;\; \text{and} \;\; s > \frac{1}{2}, \;\; \frac{m+1}{m+s} + \frac{n}{n+t} < 2, \;\; t < \frac{n+1}{m+1}s + \frac{m-n}{m+1}; \tag{5.49}$$

(Region III) $(p,q)=(0,1)$: if

$$(m,n)\notin \mathbf{V}(m,n),\ \text{ and } t>\frac{1}{2},\ t>\frac{n+1}{m+1}s+\frac{m-n}{m+1},\ 2>\frac{m}{m+s}+\frac{n+1}{n+t}; \tag{5.50}$$

(Region IV) $(p,q)=(-1,0)$: if

$$(m,n)\notin \mathbf{V}(m,n),\ \text{ and } s<\frac{1}{2},\ 2<\frac{m}{m+s}+\frac{n+1}{n+t},\ \frac{n}{m}s<t. \tag{5.51}$$

The formula for the case $m<n$ is simply obtained by switching m and n.

Note that the conditions above are all given by open sets. We do not exert any concrete conclusion when L_2, L_3 fall on the boundary of the above conditions as it seems there is no simple definite answer. See also the explanation at the end of Section 4 for the case of e_1–e_2 interfaces.

Second, subdivide the $\tilde{\kappa}_2\tilde{\kappa}_3$-plane into unit squares (5.26):

$$\mathbf{C}(m,n)=\{(\tilde{\kappa}_2,\tilde{\kappa}_3):\lfloor\tilde{\kappa}_2\rfloor=m,\ \ \lfloor\tilde{\kappa}_3\rfloor=n\},\ \ m,n\in\mathbb{N}.$$

and define $\mathbf{D}(m,n)$ to be the set formed by enlarging $\mathbf{C}(m,n)$ into the region bounded by the curves (5.29)–(5.32) and the boundaries of the rectangles $\mathbf{V}$ from $\mathbf{C}(m\pm1,n)$ and $\mathbf{C}(m,n\pm1)$. More precisely,

$$\begin{aligned}\mathbf{D}(m,n)\ &=\ \mathbf{C}(m,n)\cup(\textbf{Region III of }\mathbf{C}(m,n-1))\cup(\textbf{Region IV of }\mathbf{C}(m+1,n))\\ &\quad\ \cup(\textbf{Region I of }\mathbf{C}(m,n+1))\cup(\textbf{Region II of }\mathbf{C}(m-1,n))\end{aligned}\tag{5.52}$$

(See Fig. 27). Then for all $m,n\in\mathbb{N}$, we have

$$\mathbf{V}(m,n)\subseteq\mathbf{C}(m,n)\subseteq\mathbf{D}(m,n).$$

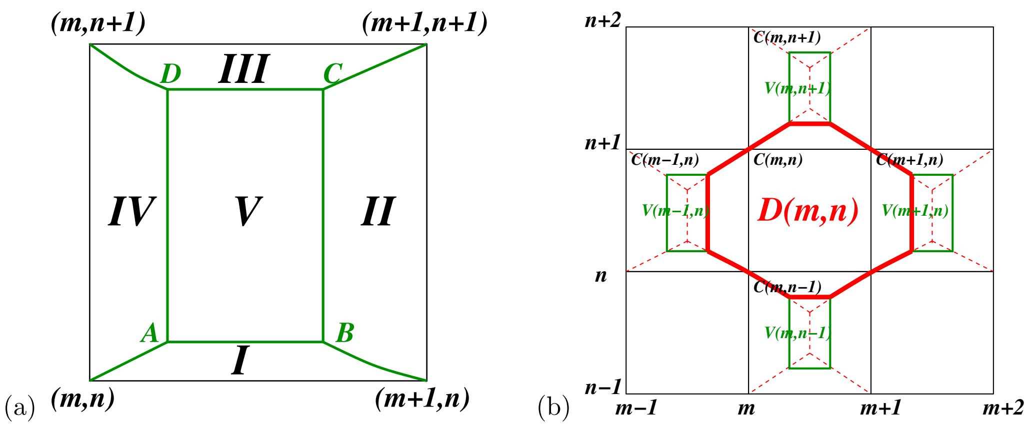

Figure 27: (a) The partitioning of $\mathbf{C}(m,n)$ into **Regions I – V**. (b) The set $\mathbf{D}(m,n)$. Note that $\mathbf{D}(m,n)$ is an enlarged version of $\mathbf{C}(m,n)$ containing part of $\mathbf{C}(m\pm1,n)$ and $\mathbf{C}(m,n\pm1)$.

Now we separate the cases depending on the type of H_3.

Suppose H_3 initially is a Type I vertex. The $\tilde{\kappa}_2\tilde{\kappa}_3$-plane is partitioned into the following sets:

$$\{(\tilde{\kappa}_2,\tilde{\kappa}_3):\tilde{\kappa}_2,\tilde{\kappa}_3\geq0\}=$$

$$\left[\bigcup_{\{(m,n):m,n\geq0,\mathrm{Par}(m+n)=0\}}\mathbf{D}(m,n)\right]\cup\left[\bigcup_{\{(m,n):m,n\geq0,\mathrm{Par}(m+n)=1\}}\mathbf{V}(m,n)\right]\tag{5.53}$$

With the above partition, then we have the following statements about the one step dynamics.

1. If $(\tilde{\kappa}_2, \tilde{\kappa}_3) \in \mathbf{D}(m,n)$ (with $\mathrm{Par}(m+n) = 0$), the minimum values of N_2 and N_3 for f are (m,n) and the new H_3 remains Type I.
2. If $(\tilde{\kappa}_2, \tilde{\kappa}_3) \in \mathbf{V}(m,n)$ (with $\mathrm{Par}(m+n) = 1$), the minimum values of N_2 and N_3 for f are (m,n) and the new H_3 becomes Type II.

This is illustrated in Figure 28.

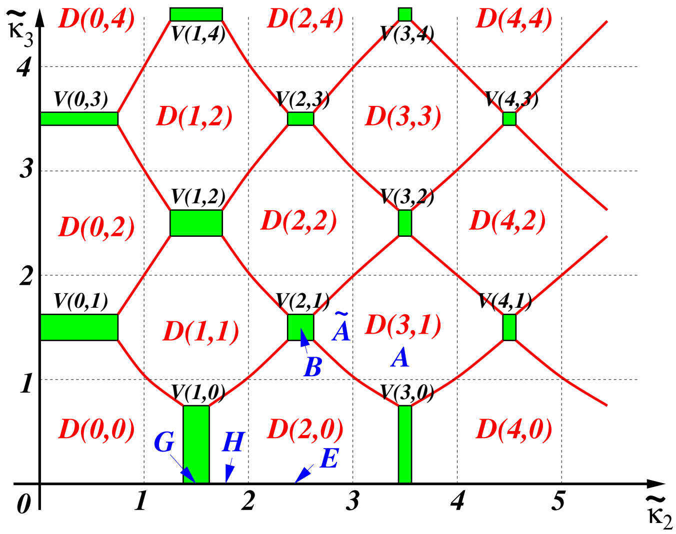

Figure 28: Starting from Type I vertex. Note that the $\tilde{\kappa}_2\tilde{\kappa}_3$-plane is partitioned into unions of $\mathbf{D}(m,n)$ (with $\mathrm{Par}(m+n) = 0$) and $\mathbf{V}(m,n)$ (shaded region with $\mathrm{Par}(m+n) = 1$). For $(\tilde{\kappa}_2, \tilde{\kappa}_3) \in \mathbf{D}(\cdot,\cdot)$, H_3 remains Type I; For $(\tilde{\kappa}_2, \tilde{\kappa}_3) \in \mathbf{V}(\cdot,\cdot)$, H_3 is changed to Type II. At point A, the vertex H_3 will remain Type I; At point B, the vertex H_3 will toggle between Types I and II. Points E, G and H represent an infinitely long finger with L_3 and L_6 equal to infinity (see Fig. 30). At E and H, the vertex H_3 will remain Type I. At G, the vertex H_3 will toggle between Types I and II.

Suppose H_3 initially is a Type II vertex. The description is very similar, except that the parity conditions for the definition of $\mathbf{D}$ and $\mathbf{V}$ are switched. Precisely, the $\tilde{\kappa}_2\tilde{\kappa}_3$-plane is partitioned as:

$$\{(\tilde{\kappa}_2, \tilde{\kappa}_3) : \tilde{\kappa}_2, \tilde{\kappa}_3 \geq 0\} = \left[\bigcup_{\{(m,n):m,n\geq 0,\mathrm{Par}(m+n)=1\}} \mathbf{D}(m,n)\right] \cup \left[\bigcup_{\{(m,n):m,n\geq 0,\mathrm{Par}(m+n)=0\}} \mathbf{V}(m,n)\right] \tag{5.54}$$

Then the one-step dynamics is given by:

1. if $(\tilde{\kappa}_2, \tilde{\kappa}_3) \in \mathbf{D}(m,n)$ (with $\mathrm{Par}(m+n) = 1$), the new H_3 is changed to Type I.
2. if $(\tilde{\kappa}_2, \tilde{\kappa}_3) \in \mathbf{V}(m,n)$ (with $\mathrm{Par}(m+n) = 0$), the new H_3 remains Type II.

This is illustrated in Figure 29.

With the above, we have the following scenarios about the transition between Type I and Type II vertices during dynamics.

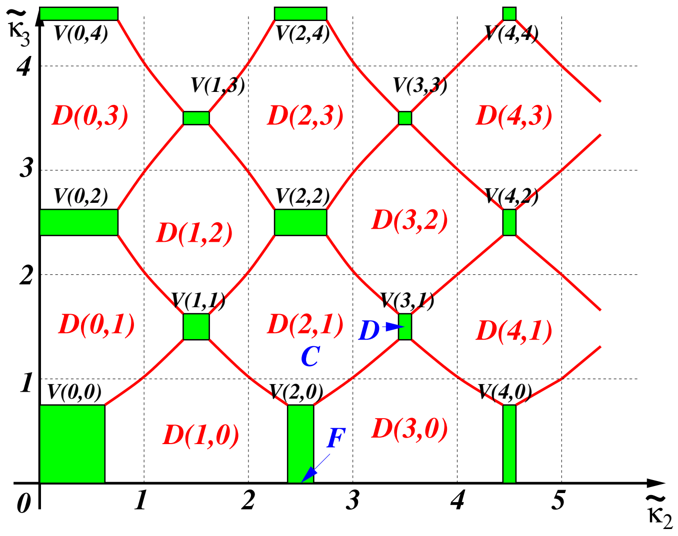

Figure 29: Starting from Type II vertex. Note that the $\tilde{\kappa}_2\tilde{\kappa}_3$-plane is partitioned into unions of $\mathbf{D}(m,n)$ (with $\mathrm{Par}(m+n)=1$) and $\mathbf{V}(m,n)$ (shaded region with $\mathrm{Par}(m+n)=0$). For $(\tilde{\kappa}_2,\tilde{\kappa}_3)\in\mathbf{D}(\cdot,\cdot)$, H_3 is changed to Type I; For $(\tilde{\kappa}_2,\tilde{\kappa}_3)\in\mathbf{V}(\cdot,\cdot)$, H_3 remains Type II. At point C, the vertex H_3 will switch to Type I and then the situation follows that of Figure 28; At point D, the vertex H_3 will remain Type II. Point F represents an infintely long finger with L_3 and L_6 equal to infinity (see Fig. 30). The vertex H_3 will remain Type II.

Starting from Type I. We are in the situation of Figure 28. Note that during dynamics, $(L_2(t),L_3(t))$ and consequently $(\tilde{\kappa}_2(t),\tilde{\kappa}_3(t))$ (defined in (5.24), (5.25)) are continuous functions of time. Hence, if initially $(\tilde{\kappa}_2(0),\tilde{\kappa}_3(0))\in\mathrm{int}(\mathbf{D}(m,n))$ for $\mathrm{Par}(m+n)=0$, then for some time interval, $(\tilde{\kappa}_2(t),\tilde{\kappa}_3(t))$ will still be inside the same $\mathrm{int}(\mathbf{D}(m,n))$. Then the minimum will be given by (m,n) with $\mathrm{Par}(m+n)=0$. Thus, during this time interval H_3 will remain Type I. (See for example point A in Figure 28.)

On the other hand, if $(\tilde{\kappa}_2(0),\tilde{\kappa}_3(0))\in\mathrm{int}(\mathbf{V}(m,n))$ for $\mathrm{Par}(m+n)=1$, then H_3 will switch to Type II in the first time step and we will be in the situation of Figure 29. In this case, H_3 will be switched back to Type I in the second step. In other words, H_3 will *toggle* between Type I and II for some time interval. See for example point B in Figure 28.

Starting from Type II. The reasoning is very similar but we are now in the situation of Figure 29. If initially $(\tilde{\kappa}_2(0),\tilde{\kappa}_3(0))\in\mathrm{int}(\mathbf{D}(m,n))$ for $\mathrm{Par}(m+n)=1$, then H_3 will be switched to Type I within one time step and then the previous case applies: it will either remain Type I or toggle between Type I and II. See for example point C in Figure 29.

On the other hand, if initially $(\tilde{\kappa}_2(0),\tilde{\kappa}_3(0))\in\mathrm{int}(\mathbf{V}(m,n))$ for $\mathrm{Par}(m+n)=0$, then H_3 will remain Type II for some time interval. See for example point D in Figure 29.

Note that it is not possible for a Type I vertex to be changed to Type II and remain Type II as $\mathbf{V}(m_1,n_1)\bigcap\mathbf{V}(m_2,n_2)=\emptyset$ for $\mathrm{Par}(m_1+n_1)=0$ and $\mathrm{Par}(m_2+n_2)=1$.

5.2.4 Formula for the Limiting Velocity Functions

From the previous section, the *one step horizontal displacements* N_2^{**}, N_3^{**} for the segments H_2H_3 and H_3H_4 are given by:

$$(N_2^{**}, N_3^{**}) = \begin{cases} (\lfloor\tilde{\kappa}_2\rfloor, \lfloor\tilde{\kappa}_3\rfloor) & \text{if} \quad H_3 \text{ is Type I and } \mathrm{Par}(\lfloor\tilde{\kappa}_2\rfloor + \lfloor\tilde{\kappa}_3\rfloor) = 0 \\ (5.47)\text{–}(5.51) & \text{if} \quad H_3 \text{ is Type I and } \mathrm{Par}(\lfloor\tilde{\kappa}_2\rfloor + \lfloor\tilde{\kappa}_3\rfloor) = 1 \\ (\lfloor\tilde{\kappa}_2\rfloor, \lfloor\tilde{\kappa}_3\rfloor) & \text{if} \quad H_3 \text{ is Type II and } \mathrm{Par}(\lfloor\tilde{\kappa}_2\rfloor + \lfloor\tilde{\kappa}_3\rfloor) = 1 \\ (5.47)\text{–}(5.51) & \text{if} \quad H_3 \text{ is Type II and } \mathrm{Par}(\lfloor\tilde{\kappa}_2\rfloor + \lfloor\tilde{\kappa}_3\rfloor) = 0. \end{cases} \tag{5.55}$$

Note that in all the cases, $N_2^{**} = N_2^*$ or $N_2^* \pm 1$ and $N_3^{**} = N_3^*$ or $N_3^* \pm 1$.

The above leads to the following formula for the velocities V_2 and V_3 in the continuum limit.

Starting from H_3 being Type I. If

(i): $\mathrm{Par}(\lfloor\tilde{\kappa}_2\rfloor + \lfloor\tilde{\kappa}_3\rfloor) = 0$; or **(ii)**: $\mathrm{Par}(\lfloor\tilde{\kappa}_2\rfloor + \lfloor\tilde{\kappa}_3\rfloor) = 1$ and $(\tilde{\kappa}_2, \tilde{\kappa}_3) \in \mathbf{V}(\lfloor\tilde{\kappa}_2\rfloor, \lfloor\tilde{\kappa}_3\rfloor)$, then

$$V_2 = \frac{1}{\alpha\sqrt{2}}\lfloor\tilde{\kappa}_2\rfloor, \;\; V_3 = \frac{1}{\alpha\sqrt{2}}\lfloor\tilde{\kappa}_3\rfloor. \tag{5.56}$$

In case **(i)**, H_3 will remain Type I (see for example, point A in Figure 28), while in case **(ii)**, H_3 will toggle between Type I and Type II (see for example, point B in Figure 28). Note that V_2 and V_3 are functions of $\tilde{\kappa_2}$ and $\tilde{\kappa_3}$ only; i.e., they are *decoupled*.

If **(iii)**: $\mathrm{Par}(\lfloor\tilde{\kappa}_2\rfloor + \lfloor\tilde{\kappa}_3\rfloor) = 1$ and $(\tilde{\kappa}_2, \tilde{\kappa}_3) \notin \mathbf{V}(\lfloor\tilde{\kappa}_2\rfloor, \lfloor\tilde{\kappa}_3\rfloor)$, then

$$V_2 = \frac{1}{\alpha\sqrt{2}}(\lfloor\tilde{\kappa}_2\rfloor + p), \;\; V_3 = \frac{1}{\alpha\sqrt{2}}(\lfloor\tilde{\kappa}_3\rfloor + q), \tag{5.57}$$

where $(p, q) \in \{(0, \pm 1), (\pm 1, 0)\}$ are determined from (5.48)–(5.51). H_3 will remain Type I (see for example, point $\widetilde{\mathrm{A}}$) in Figure 28). Note that now V_2 and V_3 are *coupled*, through the functions p and q.

Starting from H_3 being Type II. If

(iv): $\mathrm{Par}(\lfloor\tilde{\kappa}_2\rfloor + \lfloor\tilde{\kappa}_3\rfloor) = 1$, or **(v)**: $\mathrm{Par}(\lfloor\tilde{\kappa}_2\rfloor + \lfloor\tilde{\kappa}_3\rfloor) = 0$ and $(\tilde{\kappa}_2, \tilde{\kappa}_3) \notin \mathbf{V}(\lfloor\tilde{\kappa}_2\rfloor, \lfloor\tilde{\kappa}_3\rfloor)$,

then *within one step*, the vertex will become Type I and the previous case applies (see for example point C in Figure 29). Hence, these two cases will not affect the formula in the continuum limit.

If **(vi)**: $\mathrm{Par}(\lfloor\tilde{\kappa}_2\rfloor + \lfloor\tilde{\kappa}_3\rfloor) = 0$ and $(\tilde{\kappa}_2, \tilde{\kappa}_3) \in \mathbf{V}(\lfloor\tilde{\kappa}_2\rfloor, \lfloor\tilde{\kappa}_3\rfloor)$, then

$$V_2 = \frac{1}{\alpha\sqrt{2}}\lfloor\tilde{\kappa}_2\rfloor, \;\; V_3 = \frac{1}{\alpha\sqrt{2}}\lfloor\tilde{\kappa}_3\rfloor, \tag{5.58}$$

and H_3 will remain Type II (see point D in Figure 29).

We remark that in all of the cases, the velocities in the continuum limit are given by (5.56) (or (5.58)) except when H_3 is of Type I and if $\mathrm{Par}(\lfloor\tilde{\kappa}_2\rfloor + \lfloor\tilde{\kappa}_3\rfloor) = 1$ and $(\tilde{\kappa}_2, \tilde{\kappa}_3) \notin \mathbf{V}(\lfloor\tilde{\kappa}_2\rfloor, \lfloor\tilde{\kappa}_3\rfloor)$, then the velocity is given by (5.57).

Though the above description of the velocity functions involves quite a large number of cases and scenarios, in fact they can be conveniently stated in terms of the the "inverse velocity functions" $\left\{V_2^{-1}(m)\right\}_{m\geq 0}$ and $\left\{V_3^{-1}(n)\right\}_{n\geq 0}$ which partition the $\kappa_2\kappa_3$-plane into vertical and horizontal bands. See the statement of Theorem 2.10.

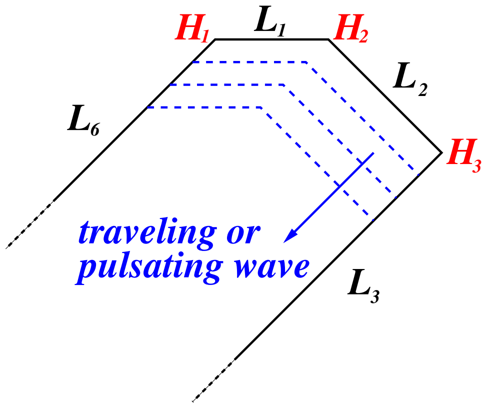

Figure 30: An infinitely long finger with L_3 and L_6 equal to infinity. Vertex H_3 can remain Type I, Type II or toggle between them.

5.2.5 An Example of an Infinitely Long Finger

Here we consider an example of an *infinitely long finger* pointing to the bisectrix direction with L_3, $L_6 = \infty$ (see Fig. 30). Then we have $\tilde{\kappa}_3$, $\tilde{\kappa}_6 = 0$ for all time and hence $(\tilde{\kappa}_2, \tilde{\kappa}_3)$ will always lie on the $\tilde{\kappa}_2$-axis. Now the dynamics is completely determined by that of L_1 and L_2. For each step of discrete time minimization, the optimal values of N_1 and N_2 are given by:

$$N_1^* = \lfloor \tilde{\kappa}_1 \rfloor \quad \text{and} \quad N_2^{**} = \lfloor \tilde{\kappa}_2 \rfloor + p_2 \tag{5.59}$$

where $p_2 \in \{-1, 0, 1\}$ and its value depends on whether $(\tilde{\kappa}_2, 0) \in \mathbf{C}(\lfloor \tilde{\kappa}_2 \rfloor, 0)$ or $\mathbf{V}(\lfloor \tilde{\kappa}_3 \rfloor, 0)$.

Upon choosing L_1 and L_2 appropriately, it is possible to have a *traveling wave* in the sense that $L_1(t) \equiv L_1$ and $L_2(t) \equiv L_2$ for all time. Then we have the following cases.

1. H_3 is Type I and $\tilde{\kappa}_2 \in \mathbf{C}(m, 0)$ for some m even in Figure 28. (See for example point E in Figure 28.)

2. H_3 is Type I and $\tilde{\kappa}_2 \in \mathbf{C}(m, 0) \backslash \mathbf{V}(m, 0)$ for some m odd in Figure 28. (See for example point H in Figure 28.)

3. H_3 toggles between Type I and Type II and $\tilde{\kappa}_2 \in \mathbf{V}(m, 0)$ in Figure 28 for m odd. (See for example point G in Figures 28.)

4. H_3 is Type II and $\tilde{\kappa}_2(t) \in \mathbf{V}(m, 0)$ for m even in Figure 29. (See for example point F in Figure 29.)

The inward normal velocity V_1 for L_1 is given by

$$V_1 = \frac{1}{\alpha} \lfloor \tilde{\kappa}_1 \rfloor , \tag{5.60}$$

while the inward normal velocity V_2 for L_2 is given by

$$V_2 = \frac{1}{\alpha\sqrt{2}} \lfloor \tilde{\kappa}_2 \rfloor \quad \text{in cases 1, 3, 4 and} \tag{5.61}$$

$$V_2 = \frac{1}{\alpha\sqrt{2}} (\lfloor \tilde{\kappa}_2 \rfloor \pm 1) \quad \text{in case 2} \tag{5.62}$$

where $\pm$ equals $+$ if (5.49) is true and $-$ if (5.51) is true.

The traveling wave solution in case 3 in which H_3 toggles between Type I and Type II should be more appropriately called a *pulsating wave* solution as the pattern changes periodically in time. But this phenomenon is only be revealed during the discrete minimization procedure. Its effect disappears upon taking the continuum limit.

Acknowledgement. The authors would like to thank the hospitality of the Institute for Mathematics and Its Applications (IMA), Minnesota, it was where this project started. The third author also appreciates the hosting by the Dipartimento di Matematica, Università degli Studi di Roma Tor Vergata of his several visits which facilitated the completion of this project.

References

[1] R. Alicandro, A.Braides, and M.Cicalese. Phase and anti-phase boundaries in binary discrete systems: a variational viewpoint. *Netw. Heterog. Media* **1** (2006), 85–107.

[2] S. Allen, J. Cahn, A microscopic theory for antiphase boundary motion and its application to antiphase domain coarsening, *Acta Metall.* **27** (1979), 1084–1095.

[3] F. Almgren and J.E. Taylor. Flat flow is motion by crystalline curvature for curves with crystalline energies. *J. Differential Geom.* **42** (1995), 1-22.

[4] F. Almgren, J.E. Taylor, and L. Wang. Curvature driven flows: a variational approach. *SIAM J. Control Optim.* **50** (1983), 387-438.

[5] L. Ambrosio, N. Gigli and G. Savaré. *Gradient Flows in Metric Spaces and in the Space of Probability Measures.* Lectures in Mathematics ETH, Zürich. Birkhhäuser, Basel (2008).

[6] N. Ansini, A. Braides, V. Chiadò Piat, Gradient theory of phase transitions in composite media. *Proc. Royal Soc. Edin.* **133A** (2003), 265–296.

[7] A. Braides. *Γ-convergence for Beginners.* Oxford University Press, Oxford, 2002.

[8] A. Braides. *Local Minimization, Variational evolution and Gamma-convergence.* Lecture Notes in Math. **2094**, Springer Verlag, Berlin, 2014.

[9] A. Braides and M. Cicalese. Interfaces, modulated phases and textures in lattice systems. Preprint, 2015.

[10] A. Braides, M.S. Gelli, and M. Novaga. Motion and pinning of discrete interfaces. *Arch. Ration. Mech. Anal.* **95** (2010), 469–498.

[11] A. Braides and G. Scilla. Motion of discrete interfaces in periodic media. Interfaces Free Bound. **15** (2013), 451–476.

[12] A. Braides and M. Solci. Motion of discrete interfaces through mushy layers. *J. Nonlinear Sci.*, to appear.

[13] L.A. Caffarelli and R. de la Llave. Interfaces of Ground States in Ising Models with Periodic Coefficients. *J. Stat. Phys.* **118** (2005), 687–719.

[14] J. W. Cahn, E. S. Van Vleck, Quadrijunctions do no stop two-dimensional grain growth. *Scipta Mater.* **34** (1996), 909–912.

[15] J. W. Cahn, E. S. Van Vleck, On the co-existence and stability of trijunctions and quadrijunctions in a simple model. *Acta Mater.* **47** (1999), no. 18, 4627–4639.

[16] X. Chen, Generation and propagation of interfaces for reaction-diffusion equations. *J. Diff. Eqns.* **96** (1992), 116–141.

[17] A. De Masi, P. A. Ferrai, E. Presutti, Reaction-diffusion equations for interacting particle systems. *J. Stat. Phys.* **44** (1986), nos. 3/4, 589–644.

[18] A. De Masi, E. Orlandi, E. Presutti, L. Triolo, Glauber evolution with the Kac potentials. I. Mesoscopic and macroscopic limits, interface dynamics. *Nonlinearity* **7** (1994), no. 3, 633–696

[19] P. de Mottoni, M. Schatzman, Geometric Evolution of Developed Interfaces, *Trans. Amer. Math. Soc.* **347** (1995), 1533–1589.

[20] L. C. Evans, H. M. Soner, P. E. Souganidis, Phase transitions and generalized motion by mean curvature, *Comm. Pure Appl. Math.* **45** (1992), 1097–1123.

[21] G. Giacomin, J. L. Lebowitz, Phase segregation dynamics in particle systems with long range interactions. I. Macroscopic limits. *J. Stat. Phys.* **87** (1997), no. 1-2, 37–61.

[22] G. Giacomin, J. L. Lebowitz, Phase segregation dynamics in particle systems with long range interactions. II. Interface motion. *SIAM J. Appl. Math.* **58** (1998), no. 6, 1707–1729.

[23] A. Giuliani, E. H. Lieb and R. Seiringer. Formation of stripes and slabs near the ferromagnetic transition. *Comm. Math. Phys.* **331** (2014), 333–350.

[24] A. Giuliani and R. Seiringer. Periodic striped ground states in Ising models with competing interactions. Preprint, 2015.

[25] T. Ilmanen, Convergence of the Allen-Cahn equation to Brakke's motion by mean curvature, *J. Differential Geom.* **38** (1993), 417–461.

[26] M. K. Katsoulakis, P. E. Souganidis, Interacting particle systems and generalized evolution of fronts. *Arch. Rational Mech. Anal.* **127** (1994), no. 2, 133–157.

[27] M. K. Katsoulakis, P. E. Souganidis, Generalized motion by mean curvature as a macroscopic limit of stochastic Ising models with long range interactions and Glauber dynamics. *Comm. Math. Phys.* **169** (1995), no. 1, 61–97.

[28] M. K. Katsoulakis, P. E. Souganidis, Stochastic Ising models and anisotropic front propagation. *J. Statist. Phys.* **87** (1997), no. 1-2, 63–89.

[29] D. Kinderlehrer and C. Liu, Evolution of grain boundaries, *Math. Models Methods Appl. Sci.* **11** (2001), 713–729.

[30] S. Luckhaus and T. Sturzenhecker, Implicit time discretization for the mean curvature flow, *Calc. Var.* **3** (1995), 253–271.

[31] A. Magni, C. Mantegazza, M. Novaga. Motion by curvature of planar networks II. *Ann. Sc. Norm. Super. Pisa Cl. Sci.* **15** (2016), 117–144.

[32] C. Mantegazza, M. Novaga, and V. M. Tortorelli. Motion by curvature of planar networks. *Ann. Sc. Norm. Super. Pisa Cl. Sci.* **3** (2004), 235–324.

[33] L. Modica, The gradient theory of phase transitions and the minimal interface criterion, *Arch. Rat. Mech. Anal.* **98** (1987), 123-142.

[34] E. Sandier, S. Serfaty, Gamma-Convergence of Gradient Flows with Applications to Ginzburg-Landau. *Comm. Pure Appl. Math.* **57** (2004), no. 12, 1627-1672

[35] P. Sternberg, The Effect of a Singular Perturbation on Nonconvex Variational Problems, *Arch. Rat. Mech. Anal.* **101** (1988), 209–260.

[36] J.E. Taylor, Motion of curves by crystalline curvature, including triple junctions and boundary points, *Differential Geometry, Proceedings of Symposia in Pure Math.* **51** (part 1) (1993), 417-438.

[37] J.E. Taylor, J. Cahn, and C. Handwerker, Geometric Models of Crystal Growth. *Acta Metall. Mater.* **40**(1992), 1443-1474.

[38] J.E. Taylor, J. Cahn, and C. Handwerker, Mean Curvature and Weighted Mean Curvature. *Acta Metall. Mater.* **40**(1992), 1475-1485.

[39] J. E. Taylor, A variational approach to crystalline triple-junction motion. *J. Stat. Phys.* **95** (1999), no. 5-6, 1221–1244.